SANDIA REPORT
SAND2022-14860
Printed October 2022

Sandia National Laboratories

Anti-Icing Coatings using Ionomer Film Layer Structuring

Nelson S. Bell, P.I., Hannah Narcross, Ashley Bowman, Annika Jansen, Gary S. Grest and Bryce A. Thurston

Prepared by
Sandia National Laboratories
Albuquerque, New Mexico
87185 and Livermore,
California 94550

Issued by Sandia National Laboratories, operated for the United States Department of Energy by National Technology & Engineering Solutions of Sandia, LLC.

Available to DOE and DOE contractors from
U.S. Department of Energy
Office of Scientific and Technical Information
P.O. Box 62
Oak Ridge, TN 37831

Telephone: (865) 576-8401
Facsimile: (865) 576-5728
E-Mail: reports@osti.gov
Online ordering: http://www.osti.gov/scitech

Available to the public from
U.S. Department of Commerce
National Technical Information Service
5301 Shawnee Rd
Alexandria, VA 22312

Telephone: (800) 553-6847
Facsimile: (703) 605-6900
E-Mail: orders@ntis.gov
Online order: https://classic.ntis.gov/help/order-methods/

ABSTRACT

This research effort examined the application of Nafion polymers in alcohol solvents as an anti-ice surface coating, as a mixture with hydrophilic polymers and freezing point depressant salt systems. Co-soluble systems of Nafion, polymer and salt were applied using dip coating methods to create smooth films for frost observation over a Peltier plate thermal system in ambient laboratory conditions. Cryo-DSC was applied to examine freezing events of the Nafion-surfactant mixtures, but the sensitivity of the measurement was insufficient to determine frost behavior. Collaborations with the Fog Chamber at Sandia-Albuquerque, and in environmental SAXS measurements with CINT-LANL were requested but were not able to be performed under the research duration.
Since experimental characterization of these factors is difficult to achieve directly, computational modeling was used to guide the scientific basis for property improvement. Computational modeling was performed to improve understanding of the dynamic association between ionomer side groups and added molecules and deicing salts. The polyacrylic acid in water system was identified at the start of the project as a relevant system for exploring the effect of varying counterions on the properties of fully deprotonated polyacrylic acid (PAA) in the presence of water. Simulations were modeled with four different counterions, two monovalent counterions (K+ and Na+) and two divalent counterions (Ca2+ and Mg2+). The wt% of PAA in these systems was varied from ~10 to 80 wt% PAA for temperatures from 250K to 400K. In the second set of simulations, the interpenetration of water into a dry PAA film was studied for Na+ or Ca2+ counterions for temperatures between 300K and 400K.
The result of this project is a sprayable Nafion film composite which resists ice nucleation at -20 °C for periods of greater than three hours. It is composed of Nafion polymer, hydrophilic polyethylene oxide polymer and CaCl2 anti-ice crosslinker. Durability and field performance properties remain to be determined.

CONTENTS

LIST OF FIGURES

LIST OF TABLES

This page left blank

EXECUTIVE SUMMARY

This project investigated the use and modification of fluoropolymers with molecular crosslinkers to enable novel anti-icing coatings. Ice formation under extreme temperature conditions including Arctic environments have great impact on energy collection and transmission, function of equipment like sensor systems, and personnel health. This effort had the goal of producing a sprayable polymer composition for protection of these systems from the formation and adhesion of ice crystals or frost films. The research approach followed the hypothesis that fluorinated polymer systems based on alcohol soluble Nafion polymers could be mixed with hydrophilic polymers or agents as a mixed system related to the inclusion of freezing point depressant salt systems, such as NaCl, KCl, $CaCl_2$, and $FeCl_2$ materials. This approach was chosen based on the potential to generate a dynamic bonding system that exploits the hydrogen bonding between materials. Control over the association of ionic and hydrogen bonding polymers with transient polymer crosslinking compounds would inhibit the crystallization phenomena of ice nucleation and allow for rearrangement of bonding moieties to enable self-healing properties. The operational goal of self-healing was desired to provide strong cycling resistance to mechanical degradation. Compositions were evaluated using visual inspection of time to frost with a Peltier plate in ambient laboratory conditions, and CryoDSC measurements of the freezing phase transition of films cast on glass slides.

The research plan focused on the selection of crosslinking and de-icing agents for a blended icephobic system. Multiple iterations of concepts were tested, including the use of polyelectrolytes as self-healing systems, a variety of divalent salt systems, and several non-ionic hydrophilic surfactants. The timeframe to conduct the measurements led to project delays in the milestones for external testing, leaching, and adhesion testing. Primary discoveries regarding the cast films showed that cycling failure related to film thickness. Routes to improve film cohesion and subsequent cycling stability were developed by the incorporation of a glycol modified nano-clay material, or by increasing the film thickness via the use of a more concentrated precursor solution. Ultimately, a formulation was developed which demonstrated ice nucleation inhibition for a period of greater than three hours. This system has fluidity suitable for a pneumatic spray deposition approach, but the project termination date prevented demonstration of that characteristic. Self-healing was not demonstrated in the final formulation. Intellectual property related to the composition and wide application of the system is in process.

The final formulation achieved in the research effort has the potential to enable field application/repair of components in Arctic conditions. Additional verification of stability and ice adhesion is required to move toward use in arctic and high-altitude operational equipment, heat exchangers, remote or autonomous sensor and power equipment of interest to national security. The spray method capabilities are applicable to high surface area installation (over 1 m2) and retrofitting to existing infrastructure.

ACRONYMS AND TERMS

Acronym/Term	Definition
Cryo DSC	Cryogenic Differential Scanning Calorimetry
$CaCl_2$	Calcium Chloride
KCl	Potassium Chloride
$MgCl_2$	Magnesium Chloride
$FeCl_2$	Ferrous Chloride
NaCl	Sodium Chloride
PAA	Polyacrylic Acid
PEO	Polyethylene Oxide
$ZnCl_2$	Zinc Chloride
SAXS	Small Angle X-ray Scattering

1. INTRODUCTION

Ice accumulation under extreme thermal conditions such as the Arctic environment is a significant detriment to operational capabilities in energy collection and transmission, remote sensor monitoring, aircraft systems, and wind turbines. Novel capabilities are needed to increase the security and resilience of physical infrastructure and in autonomous and aircraft systems to improve domain awareness, time of operation, and asset distribution. Heating input to de-ice surfaces requires passive or active approaches, which benefit from smart device integration.[2] The process of ice accumulation on a surface is non-trivial, with multiple modes of ice formation including freezing rain, snow, and frost formation as examples. These require an understanding of multiple effects of the growth mechanism related to surface temperature, nucleation thermodynamics and kinetics, and adhesion strength.[3] An understanding of the factors that control ice adhesion remain strongly researched and discussed.[3-5] Numerous factors in ice formation are interrelated, and the formation of surface ice layers has multiple pathways.[4, 6, 7] Material coatings are highly desired to prevent or remove ice accumulation. Anti-icing approaches for surface coatings (passive systems) are focused on either nucleation inhibition, low adhesion force (adhesion stress, τ_{ice} < 20 kPa) [8, 9], or growth prevention [10] The current state of technology uses an ice prevention strategy (salt and glycol) related to wetting and adhesion science within the surface.[11] This has environmental and performance concerns that would preferrable be overcome. However, this anti-icing approach lacks durability, physical resilience, and requires expertise in installation and maintenance. A successful coating approach should be easily applied over large areas (suitable for over 1 m^2) and with durable freeze-thaw characteristics (less than 3% decrease over 100 cycles, 0 to -20 °C) to be relevant on a practical scale.

There are multiple examples of coating formulation promoted for these environments related to control over surface properties[10, 12, 13] with inspiration related to biological molecules[14-18], ice structure[19] and hydrogen bonding in water[20], surface wetting[21-23], and in the mechanical properties of coatings. To reduce adhesion energy (adhesion stress, ice < 20 kPa), low surface energy materials were identified including silicones and fluorinated films or surface treatments.[24, 25] Wetting strategies were related to the presence of surface roughness or the imposition of surface texturing.[4, 17, 26, 27] However, surface ice film formation can be based on vapor deposition and heterogeneous nucleation of ice occurs at a scale of 1 micron.[10] Stronger adhesion forces are generated under the condition of vapor based adhesion, or strong kinetic impact of freezing rain leading to complete surface wetting. Textured surfaces were improved by filling the coating with lubricant fluids, either as a swollen polymer gel or as an infusion of a textured interface.[12, 13, 28-31] However, the lubricants can require replacement, and the surfaces can require fine control over texture. The work of the Tuteja group at the University of Michigan controlled the degree of crosslinking in several polymer systems, showing that a low degree of crosslinking can create high chain mobility in a low surface energy coating.[32] This creates an elastomeric system with low surface modulus. Ice removal then becomes facile due to the elastomeric compliance of the film. Likewise, He et al. used a mixture of PDMS and hydrogel materials to tackle the primary issues of ice nucleation, ice growth, and ice adhesion.[33] This work balanced the effects of interfacial water to form a lubricating layer with the hydrophobicity of the PDMS network to lower adhesion and shows that control over -OH content and hydrophobic segments is needed to successful anti-icing properties.

Chemistries that prevent the nucleation of ice crystals are expected to enable longer time to ice nucleation, greater undercooling temperatures and faster thawing behavior. Biological systems have been surveyed to determine molecular features that can be adapted synthetically to accomplish the same goals.[14] The interplay of hydrophobic hydrocarbons, polar amide and carboxylic acid groups, molecular spacing and content establish the theme of prevention of large hydrogen bond networks as a requirement of anti-icing films. Hydrophilic polymers as a component phase of an anti-icing film have been demonstrated to act as an anti-ice crystallization phase which prevents nucleation and ice crystal adhesion to a coating. [22, 34, 35] With systems containing liquid water, hydrogels have been utilized to prevent ice crystallization, as well as exhibit elastomeric properties would favor weak adhesion strength.

[33] These types of gels can be conceptualized with self-healing properties. Self-healing properties are expected to be highly advantageous for coatings that would experience thermal cycling, impact events, or frictional use.[36] Many examples of this utilize ionic bonds within a hydrogel structure.[37, 38]

Self-healing polymer networks are formed when inter chain bonding is non-covalent, and dynamic. This flows from the concept of self-healing hydrogels, in which the cation species can move within the mobile backbone network to change bonding sites. This allows for deformation and elasticity, as used in electronic polymers.[39] The strength of bonding needs to be moderated and can be ionic or hydrogen bond related. In practice this leads to mixtures of polar chemical groups, mixed with hydrophobic alkyl groups or nonpolar chemistries. Anti Freezing Proteins (AFP) have similar base chemistries of amides, -OH groups and carboxylic acids.[33, 40, 41] A principle behind this anti-icing feature is the prevention of regions having uniform repeating units of -OH groups and the use of varying length of hydrocarbon spacers/regions, thereby frustrating the formation of ice nuclei. This same feature is needed to moderate the forces between the ionomer groups proposed here. In addition, the presence of liquid water in mixtures of polar groups can be designed to create the formation of liquid like surface layers based on ambient water based lubrication layers.[16, 22, 31, 42] Control over the strength of the interaction and the functional mobility of the network has the potential to achieve the desired goals for ice-preventative coatings suitable for the arctic environment.

The films described in literature either have complex surface structures or have fabrication requirements that need controlled conditions. These works do not address the critical problem of abrasion resistance for coated materials. Operations in arctic equipment undergo severe stress levels and environmental shocks, including aerosol abrasion in air transport. There are attempts to create large scale coatings for anti-ice performance using thermally sprayed polyethylene[43] or PTFE has been applied to prevent ice adhesion using powder particles deposited by electrostatic self assembly, followed by sintering operations.[44] Despite the headline that this is a large area deposition method, it requires specialized equipment and procedures to create the desired film, and is prohibitive to apply under field conditions. Of interest to this work was the ability to apply a film or coating during field operations using spray deposition. A method if this type would best be applied under ambient conditions with no premixing or thermal/UV crosslinking methods.

The research proposed here is to use ionomer based polymer and small molecule crosslinkers to create self healing films with low ice adhesion properties, low nucleation of frost layers, and facile application of durable films. Our approach is to utilize fluoropolymer-based ionomer films to produce an antifreezing surface in a field sprayable and repairable fashion. A sprayable formulation for a deicing coating that is effective, repairable, and simple is needed for widespread application and retrofitting to artic or polar materials use. This method is based on technologies in flexible electronics where damage tolerance and self-healing concepts have been prioritized, and biology where anti-icing proteins and damage tolerance during freezing are of interest.

1.1. Nafion material systems.

Nafion polymers are fluorinated ionomers invented by DuPont, and have significant applications as ion membranes for battery and fuel cell devices.[45] The structure of Nafion is based on the interactions between the polytetrafluorethane backbone of the polymer and the number of perfluorovinylether sidegroups. These polymers have fluorinated backbone chains with strong hydrophobicity, and side chains terminated with sulfonate groups that self-assemble into ionic domains by molecular mobility.[46] The commercial products may have molecular weight variation and variation in the spacing of sidegroups, making understanding of the packing and morphology of Nafion films and membranes a complex task. Numerous structure models have been developed and tested to fit data from USAXs, SAXS, and SANS measurements, summarized by Mauritz.[47] Common to all, are the separation of the

sulfonated groups into ionic domains, which experience swelling and uptake of solvents including water and alcohols. The percolation or interconnection of the ionic materials is expected to lead to the valuable ionic transport properties of Nafion.

Processing and structure of the polymer affects the morphology in complex ways and exhibits reversible restructuring effects based on environmental interactions. The structure of Nafion is modified by the balance of hydrophobic and polar interactions. Papers specifically studying the freezing of water in Nafion show that the freezing point of water *inside* the membrane is depressed through a combination of adsorption of "bound water" on sulfonic acid groups and the confinement of water within the nanodomains.[48-50] Nanodomain size will determine whether or not ice can form in the "pores" of the network (center of the domains) which can be pushed to the surface and freeze.[51-53] These materials already show dynamic chain properties based on surface wetting behavior.[54] The addition of binding chemistries or deicing agents/polymers is our method to alter the properties of these polymers and achieve the needed material properties.[55]

Nafion polymers are soluble under elevated pressure and temperature in alcohols, and are used to create films in electrochemical systems as separators. This provides a system in which sprayable precursors can be visualized to easily be pneumatically deposited over large areas. Nafion is shown to display hydrophobic behavior when films are sufficiently thick.[54, 56, 57] The cast films are known to create a biphasic structure, creating a nanoporous network from solution deposition.[58] Filling the interstitial space with a hydrophilic polymer is a route several studies in ion transport have taken in order to modify properties, and is similar to the bound water anti-ice systems. There is significant research in the formation of blended films with other surfactants.[59, 60] Li et al. found that a blended film of polyvinyl alcohol with Nafion demonstrated anti-fogging behavior, based on the uptake of water into the PVA network. [34] These materials required the Nafion presence to prevent water to ice formation, but the mechanism is not well understood. Finally, the sulfonic groups within Nafion are known to associate with divalent cations, including Barium, leading to changes in mechanical properties based on the electrostatic and hydration sphere of the system.[61] This provides a route to contain freezing point depressant salts based on divalent cations. Prior approaches use *hydrogen-bonding* and *hydrophobic groups* to effectively regulate interfacial water. We used this to guide our design. Mixture of hydrophobic Nafion, and hydrophilic hydrogel materials with ionomeric groups uses *salt eutectic* effects to retain mobile water in freezing conditions.

1.2. Structure of Nafion copolymer.

The application of Nafion polymers were greatly expanded upon the development of procedures to generate Nafion solutions. This process utilizes autoclave techniques at 150 °C or greater and water-alcohol mixtures to create transparent solutions.[47] The water and alcohols both demonstrate the capability to swell Nafion films, and by stabilizing the electrostatic forces from the anionic terminal groups of the side groups, and minimizing the attraction of the perfluoro backbone, soluble species are industrially produced. As these materials are electrostatically stabilized, their gelation can be induced by the addition of salts, and they have been used in the formation of composites related to electrostatic attraction to positively charged colloids.[62] Nafion solutions are not in actuality dissolved polymers, but are composed of individual chains and rod-like aggregates that are highly charged. The larger particles are believed to be structured with the hydrophobic backbone polymer chains associated into the center. Their dimension was found to be a diameter of 6 nm, with a length of > 100 nm in Rubatat et al.,[63] and a size of 50 nm or 1 micron using static light scattering.[64] The size formation can be varied by choice of solvent, and filtering of the product as well. Nonionic interactions can also be utilized in processing Nafion can engage in solvation based binding with polypropylene, as demonstrated by the specific hydrophobic attraction of Pluronic tri-block copolymers to the hydrophobic backbone of Nafion, and the formation of composite aggregates with the polypropylene component.[60] The aggregates size is

thought to be thermodynamically based into the nanosized and larger aggregates, as Cirkel et al. noted the reappearance of large aggregates after filtration and solvent evaporation. The solution assembly into films therefore involves colloidal assembly and restructuring during an evaporation process, or specific adsorption to a surface through attractive van der Waals or electrostatic interactions. The behavior of Nafion as a function of concentration in solution is modeled with interesting behavior, summarized by Mauritz and Moore,[47] with a phase inversion from an agglomeration of rods at high water fraction, to a phase inversion at a water fraction of ~50% to give a biphasic structure, and drying into a swollen membrane or ultimately the perfluorinated matrix with a distribution of ionic domains.

The surface properties of Nafion have demonstrated flexibility to the interaction environment, with the development of hydrophilic properties upon exposure to water.[54] The development of water wetting properties is based on the swelling of the ionomer domains, and inversion of the surface structure from the hydrophobic to hydrophilic species, but should not be confused with a low contact angle. Nafion develops a strong adhesion energy with water or methanol, as exhibited by a low receding contact angle, but the static contact angle still behaves as a hydrophobic interaction. The swelling of Nafion films leads to mechanical stress as well.[6] The chemical properties of Nafion surfaces have continued to show unusual properties, with surface separation dependent properties up to several hundred microns of pH, birefringent optical properties, and a higher index of refraction in the surface layer (n = 1.46).[65, 66] Bunkin et al. argue that all these properties arise from the electrostatic repulsion between the charged ionomer side groups, that cause the partial dissolution of surface Nafion chains, to form extended anisotropic rod structures perpendicular to the surface.[65] These surface potentials are up to -120 mV. These extended chains are still tethered to the surface but are ordered into a colloidal crystal matrix at the surface, with a range of hundreds of microns (~800 μm) from the surface. It is interesting to note that Cirkel et al. cited NMR results from Schlick et al. on increasing mobility of Nafion chains by NMR, and the dissolution argument is supported by the potential for partial dissolution of Nafion from the swollen polymer surface.[64, 67]

1.3. Anti Ice Film Development Plan

We will test several compounds for the capability to create these novel films based on surface wetting, anti-ice formation properties, and self healing capability. The chemical variations to be tested involve the choice of additives that create the anti-icing properties of the surface. The materials identified can be classified as:

a) Ionic Salt Compounds: the use of anti-freeze salts was explored for their intrinsic freezing point depression effect as well as their impact on crosslinking of the sulfonate groups in Nafion. Deicing salts like $CaCl_2$ and $MgCl_2$ are common approaches to reducing the freezing point of water. These are characterized by the van't Hoff factor (*i*) and the concentration of the salt in aqueous solution.

$$\Delta T_f = imK_f$$

The van't Hoff equation uses the molar concentration, *m*, the van't Hoff factor (*i*), and the freezing point depression constant K_f (a property of the solvent, 1.86 °C/*m* for water) to determine the effect of added salt. The ideal number I would correspond to the number of ions produced by the dissociated salt, giving 3 for $CaCl_2$ for example. However, ion pairing causes deviation of these values. Measured values provide a scale for comparison of the ability of salt solutions to lower the freezing point of water.

Our interest was to use freezing point depression factors in common de icing salts $MgCl_2$ and $CaCl_2$, and examine the effect of ion properties using $ZnCl_2$ and $FeCl_2$. Table 1 tabulates values for freezing point depression of increasing molar concentrations of salt solutions.

Table 1. Freezing Point Lowering for Aqueous Solutions (CRC Handbook, 86th Edition).

Compound	0.5 m	1.0 m	2.0 m	3.0 m
NaCl	1.68			
KCl	0.17	3.29	6.50	9.77
$MgCl_2$	2.31		2.7	3.0
$CaCl_2$	2.66	6.35	15.27	28.08

b) Hydrophillic Polymer Surfactants: In the course of the research, several hydrophilic surfactants were considered for addition to Nafion solutions to form hybrid films. These include several polyethylene glycol surfacants, including hydroxyl terminated, methyl ether termination, and naphthalene derivatives (Solsperse 27000). Disperbyk-190 is a low molecular weight polyacrylic acid which was tested as well. Modification of polyacrylic acid to improve alcohol solubility was attempted as well.[68]

c) Colloidal Nanomaterials: the addition of solid nanoparticles like clays, graphene oxide, or polymer spheres can change the tortuosity, moderate physical properties with temperature, and improve damage tolerance and surface wetting. In this project, we utilized glycoboehmite nanoflakes for reinforcement of the dip coated films. Figure 1 provides a micrograph of these materials, as detailed in published work. These materials were developed at Sandia-Albuquerque in cooperation with Ed Matteo (8842) for study of unique ion binding for environmental remediation.

The synthesis and structure of glycoboehmite materials are presented in a recent publication by Bell et al.,[69] finding that flakes of glycoboehmite are easily synthesized with surfaces terminated with glycol molecules. Figure 1 provides a micrograph of these materials, as detailed in published work. It was reasoned that these flakes would have high surface area, platelet reinforcing activity, and potentially incorporate the anti-freeze properties of the glycol surfaces into the film. Additionally, the index of refraction of these materials is near 1.52, making it possible to lower light scattering effects for transparency.

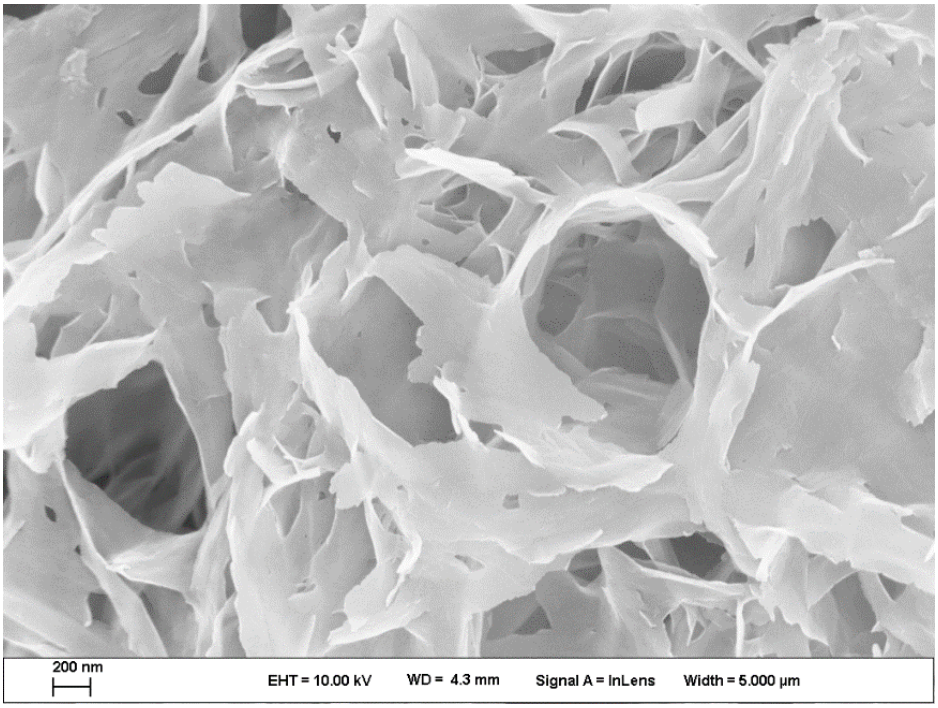

Figure 1. Scanning Electron Micrograph of glycoboehmite nanoflakes used in film reinforcement.[69]

These precursors have the potential to intermix with other compounds having improved antiwetting properties, interpolymer attraction, and hydrogen bonding to generate the desired self-healing films.

For this work, we will conduct chemical synthesis and incorporation of binding agent chemistry in order to alter and ultimately tailor the behavior of the Nafion polymers. Computational modeling will be utilized to determine the binding strength of crosslinking additives and the expression of surface properties related to ice nucleation and adhesion. Coatings will be measured for their physical, thermal, and surface wetting properties using methods including glass transition temperature and melting point, hardness (T), water contact angle, and ice formation temperature, and ice adhesion stress. The films will be tested for resistance to damage by aerosols, and also physically abraded to induced surface damage, thereby characterizing their tolerance for real world applications. Finally, the films will be evaluated for self healing and self repair when treated thermally or with solvent. The best candidate agents for modifying properties will be examined for further optimization in FY22.

2. MATERIALS AND METHODS FOR NAFION COMPOSITE FILMS

2.1. Materials and Chemicals

Nafion Dispersion D2020 was purchased from FuelCellStore as a 20 wt. % dispersion in a 35/45 wt. % 1-propanol/water mixture. 1-Propanol (99.5%), poly(ethylene glycol) (PEG), poly(ethylene glycol) methyl ether (PEG-Me), poly(vinyl alcohol) (PVA), poly(acryclic acid), hexadecanol, dopamine hydrochloride, iron chloride, calcium chloride, magnesium chloride, and zinc chloride were obtained from Sigma-Aldrich and used without further purification. Calcium chloride was obtained from EM Science and used without further purification. Glass microscope slides (25 mm × 75 mm), used for ice-nucleation frost tests, were obtained from VWR Avantor North America.

2.2. Solution Preparation

Nafion D2020 was used neat or diluted down to a 5 wt. % solution in a 35/45 wt. % 1-propanol/water mixture. 20 wt. % solutions of anti-icing agents (dopamine-HCl, PVA, PEG, and PEG-Me) were prepared in a 35/45 wt. % 1-propanol/water mixture. Dip-coating solutions were prepared by mixing Nafion and anti-icing agent solutions at room temperature for 30 minutes. For crosslinked solutions prepared with un-diluted Nafion D2020, calcium chloride was directly added into the respective solutions in a 1:10 calcium chloride to Nafion ratio and sonicated for 20 minutes. For crosslinked solutions prepared with diluted Nafion D2020, dip-coated films were soaked in aqueous ionic salt solution (1M) for 10 min after which the films were dried under ambient conditions.

2.3. Film Preparation

Glass slides were cleaned with ethanol and DI water, then plasma cleaned (Plasma Etch PE-75) for 2 minutes. Dip-coating solutions were then separately poured into 50mL beakers, and the glass slides were partially immersed for 10 minutes and slowly removed. The partially-coated slides were then taped to a petri dish to dry horizontally either at ambient conditions overnight or in a 90 ^{o}C oven for 30 minutes.

2.4. Characterization

Ice-nucleation on the coatings were examined by placing coated slides on a Peltier plate, temperature controlled by Leica Vibratome State Freezing Stage. The Peltier plate was initially stabilized at 25^{o}C and brought down to -20^{o}C. After visible ice-nucleation appeared the Peltier plate was brought back up to 25^{o}C. This cycle was repeated over two-seven trials. Surface hydrophobicity was measured using VCA Optima Coast Products contact angle analyzer with a 2.0 µL drop of water. Contact angle was measured as the average of three tests over various portions of the coated film. The coating thickness and roughness was measured by a DektakXT Bruker profilometer. Profilometry was measured using a range of 65.5 µm, a length between 2000-5000 µm, a duration of 10 seconds, and a stylus force of 1 mg. DSC measurements were conducted on a DSC-Q200 differential scanning calorimeter. Before and after ice-nucleation pictures were taken on VHX-7100 optical microscope from Keyence.

3. RESULTS AND DISCUSSION

3.1. Baseline Behavior

Initial frost tests were performed on unmodified dip-coated Nafion films (with thicknesses in the range of 3-14 µm measured via profilometry) deposited on O_2 plasma-treated glass substrates (Figure 2) and dried at room temperature (RT) or 90 °C in order to establish the baseline behavior of the system. Nafion films as deposited were highly transparent which made it simple to visually distinguish when the uncoated glass had been covered in frost as well as when frost formed on the surface of the film (Figure 3). Initially, Nafion films delayed frost formation from ~1 min (uncoated glass) to ~14:30 minutes and ~5:45 minutes when dried at RT and 90 °C respectively. However, time-to-frost (TTF) decreased with subsequent heat/cool cycling until matching or only marginally improving the TTF of untreated glass by the 7th trial. Subsequent efforts focused on improving the TTF time and stability of Nafion films as well as determining the cause for the loss of performance over time.

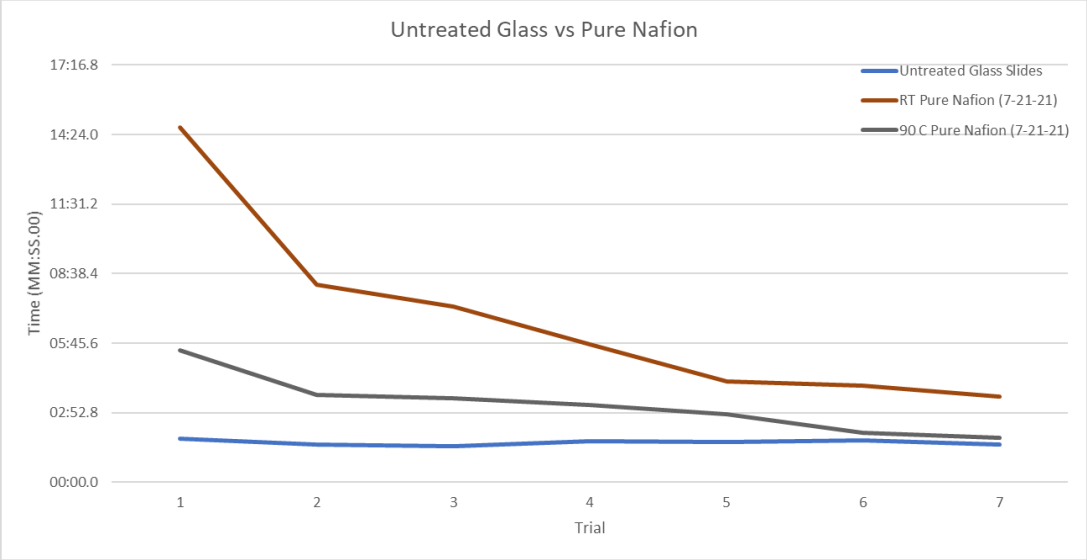

Figure 2. Time to frost formation on dip-coated Nafion films dried at RT or 90 °C and on uncoated glass. After frost formation was observed, the partially coated slide was allowed to warm to room temperature and the test was repeated a total of 7 times (Trials 1-7).

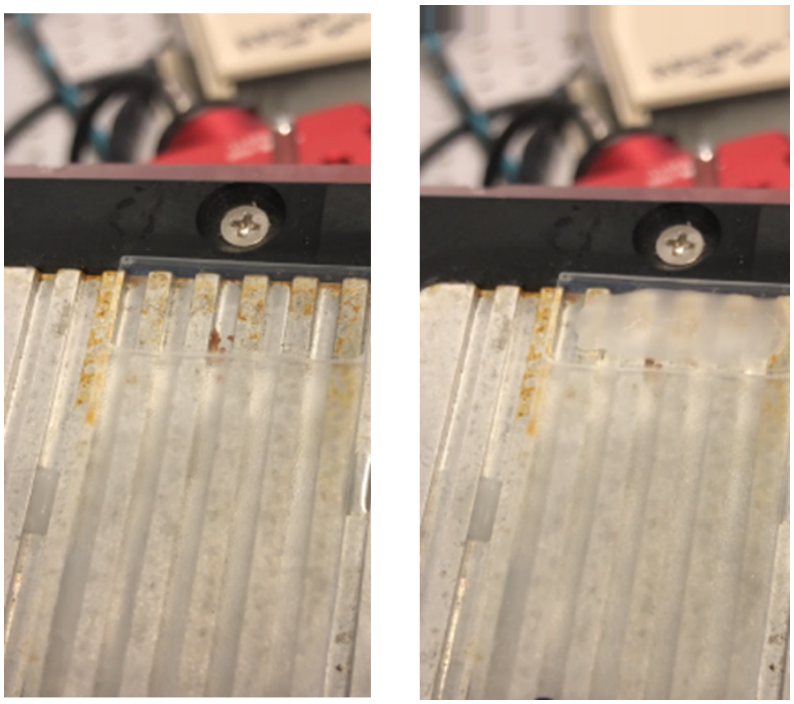

Figure 3. Dip-coated Nafion film on glass slide during frost testing on Peltier plate. (Left) Initially the coated (upper) portion of the slide remains transparent prior to frost formation while the lower uncoated glass portion has frosted over and become opaque/hazed. (Right) Onset of frost formation on the Nafion film can be visually observed by formation of opaque/hazy ice surface layer.

3.2. Nafion Films Blended with Anti-freezing Agents

Nafion films self-assemble into a microphase separated hydrophobic perfluoroalkyl ether matrix imbedded with a continuous network of hydrophilic domains. These hydrophilic domains are composed of sulfonic acid groups from the Nafion polymer side-chains and absorbed liquid water. Nafion dispersions were blended with varying amounts of three different low molecular weight poly(ethylene glycols) (PEGs) that differed in their end groups. These were hydroxyl terminated poly(ethylene glycol) (PEG, Mn 400), poly(ethylene glycol) methyl ether (PEG-Me, Mn 550), and naphthalene terminated poly(ethylene glycol) sold commercially as Solsperse-27000 (PEG-Nap). PEGs are well known in the literature to inhibit ice formation by interrupting hydrogen bonding of water, and it was expected that they would segregate to the hydrophilic domains in Nafion films and inhibit or prevent the freezing of the absorbed liquid water within the domains. An alternative antifreezing agent (partially alkyl-functionalized poly(acrylic acid) (PAA)) was also briefly explored (Figure 4).[68] The motivation for this was the expectation that segregated antifreezing agents had a possibility of leaching out of the system over time, and that hydrophobic alkyl side-chains might integrate into the hydrophobic matrix to prevent this. However, even at low levels of functionalization (5%) the modified PAA was rendered insoluble in the 35/45 (by weight) 1-propanol/water mixture that the Nafion D2020 is dispersed in. Therefore this was not explored further. A high molecular weight block copolymer commercially sold as DISPERBYK-190 as a wetting and dispersive additive for aqueous systems was also explored.

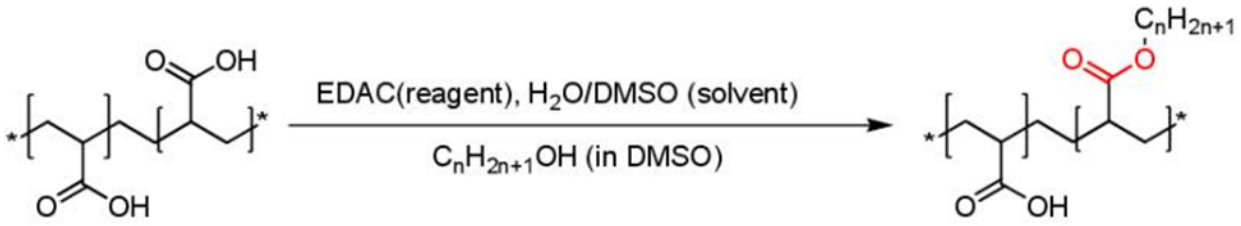

Figure 4. Scheme for preparing partially alkyl-functionalized poly(acrylic acid).

Blending Nafion with antifreezing agents was expected to improve TTF times and stability through a combination of inhibiting the nucleation of ice crystals that would provide nucleation points for frost to form on the surface of the film as well as inhibiting water freezing within the film which is known to increase the Young's modulus and cause films to become more brittle. The TTF results for these blends are summarized in Figure 5 and Figure 6.

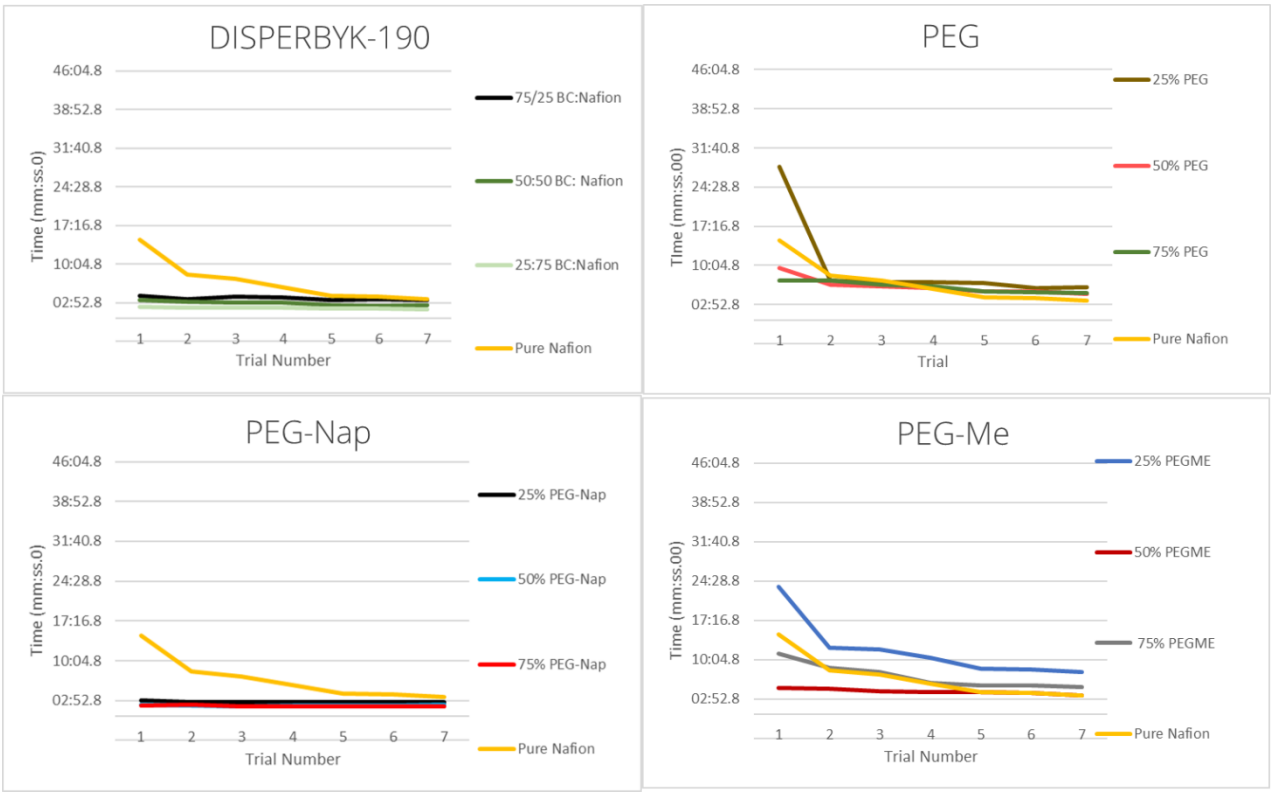

Figure 5. TTF for blended Nafion films dried at RT. Reported amounts are relative volumes of 20 wt.% solution of antiicing agent to 5 wt.% Nafion dispersion which were combined and used as dip-coating solutions to deposit films.

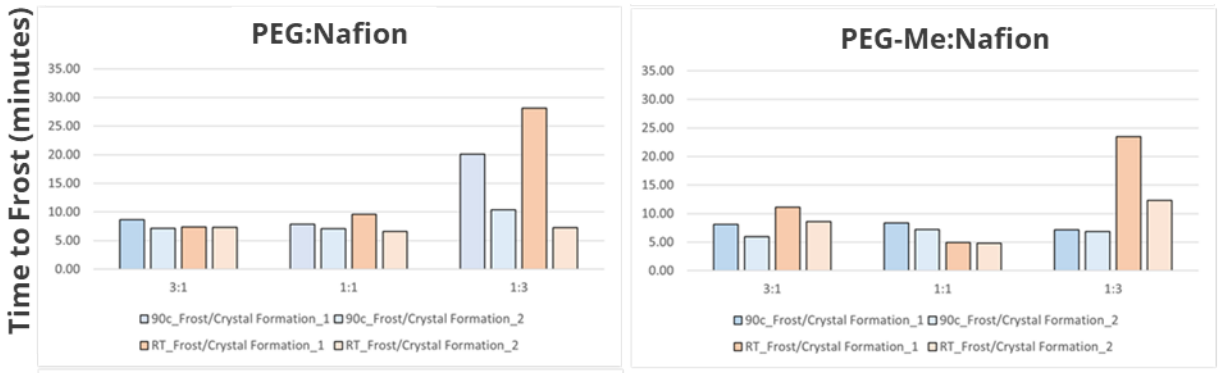

Figure 6. TTF for Nafion/PEG and Nafion/PEG-Me blended films reported as ratio by vol. of PEG/PEG-ME solution (20 wt.%) to Nafion (5 wt.%) used to for dip-coating solutions. 1 and 2 refer to the first and second freeze/thaw cycle respectively.

The addition of PEG-Nap and DISPERBYK-190 showed little to no effect on TTF at all levels tested; in fact TTFs were lowered compared to neat Nafion films dried at RT. The addition of PEG and PEG-Me at 3:1 and 1:1 also showed little to no difference from the performance of neat Nafion film. However, when added at loading levels of 3:1 the TTF of the first freeze/thaw cycle was noticeably improved for films prepared with both PEG and PEG-Me. Notably the TTF of the 3:1 Nafion:PEG blended film dried at room temperature was improved to ~27 minutes. In all cases the TTF was still observed to decrease with subsequent freeze/thaw cycles. Microscopy of the films before and after freeze tests reveals the most likely explanation for this behavior (Figure 7).

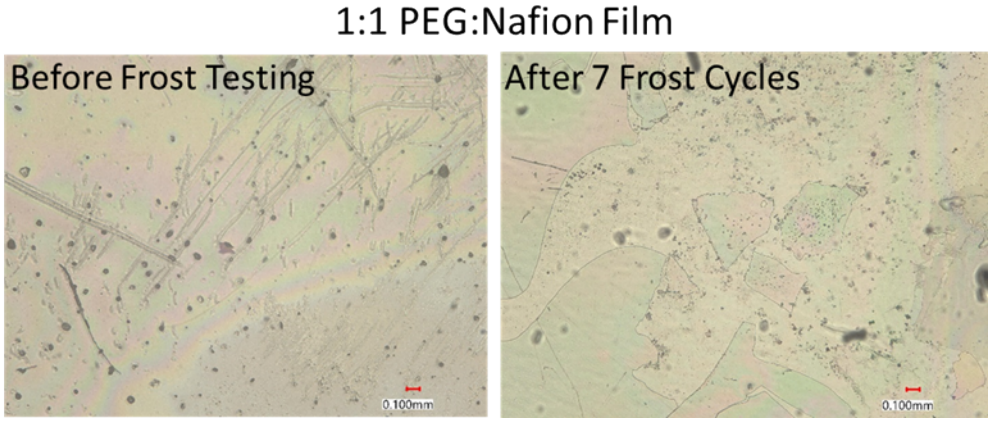

Figure 7. Optical microscopy of an exemplar blended film prepared from a 1:1 by weight Nafion and PEG dip-coating solution before and after 7 freeze/thaw cycles.

In all cases, significant damage to the films could be observed following repeated freeze/thaw cycles. The likely explanation is that the antifreezing agents were unable to entirely prevent internal water freezing when the temperature of the film was lowered to -25 °C, causing films to become more brittle. This in combination with the stresses from repeated expansion and contraction of the hydrophilic domains via the freezing and melting of adsorbed water caused the films to fracture, exposing the uncoated bare glass and increasing the roughness of the film which can accelerate frost formation by providing multiple nucleation points for ice to form.

A variety of approaches were then explored to improve the mechanical stability of the films including the inclusion of nanoclay fillers, multivalent cationic salts expected to act as crosslinkers for the negatively charged sulfonate groups, as well as dip-coating thicker more films in the hope that they would be more robust and less likely to fracture.

3.3. Nanoclay Filler

Films prepared with 5 vol.% of the nanoclay solution showed marginal improvement in film stability compared to neat Nafion films (Figure 9). After 7 freeze/thaw cycles Nafion films were catastrophically damaged such that the entirety of the film was broken into shards such as those seen in Figure 7. Films prepared with 50 vol.% clay solution showed an even greater resistance to freeze induced film damage with all films remaining cohesive and unbroken after 7 frost cycles. These results did not translate to improved TTF unfortunately which underperformed compared to neat Nafion films dried at RT (Figure 8). The exact cause for this behavior is unknown; it is unlikely that the inclusion of the nanoclay made the surface significantly more hydrophilic such that ambient water absorption/freezing was significantly accelerate especially when the results from Nafion blended films containing excess amount of hydrophilic polymers such as PEG are considered. It is possible that the nanoclay increased the surface roughness of the film and provided more ice nucleation points, although profilometry of films was unable to distinguish differences in average roughness between neat Nafion and Nafion/nano-clay films due to naturally large variations in surface thickness in the dip-coated films as well as the presence of dust and particulates in films as they were not prepared in a clean-room environment.

Regardless of the cause, nanoclays were found to improve the mechanical properties of Nafion films but decreased TTF such that they were not explored further.

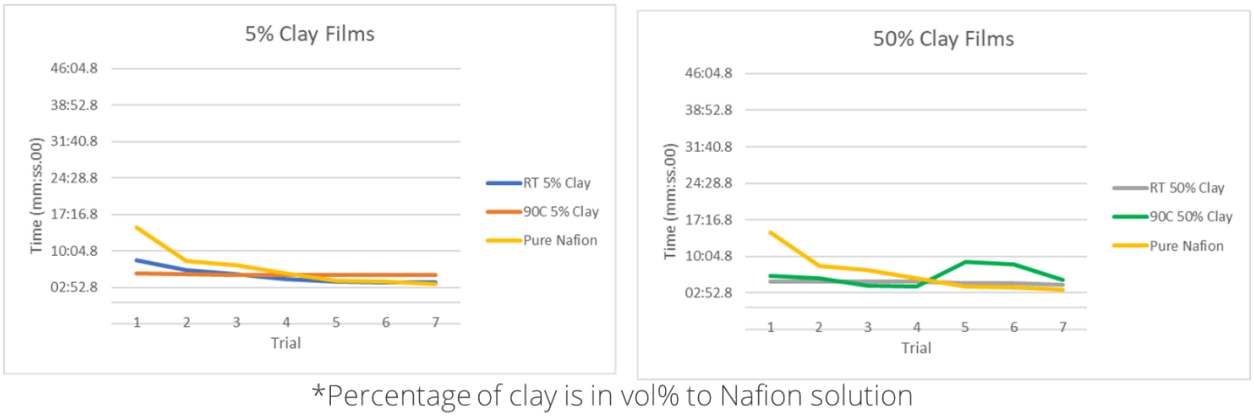

Figure 8. TTF of blended Nafion and nanoclay films prepared from a 5 wt.% dispersion of Nafion and 5 or 50 vol.% nanoclay solution (wt. % unknown)

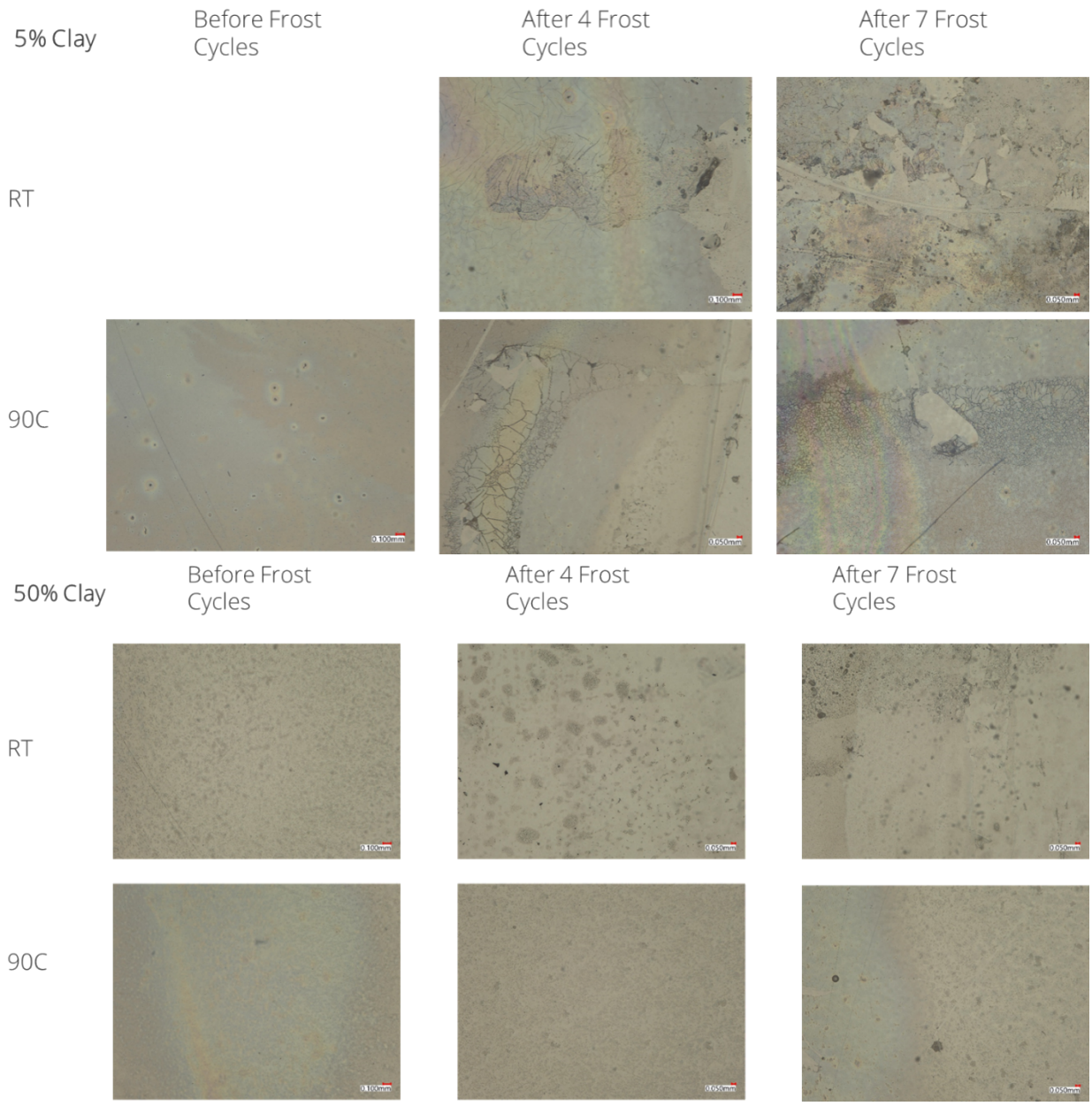

Figure 9. Optical microscopy of blended Nafion and nanoclay films.

3.4. Cationic Salt Crosslinker Screening

Self-healing properties of anti-frost/anti-ice Nafion films are important both for their long term durability as well as to prevent or heal damage that occurs in the film when absorbed water in hydrophilic domains freeze. Multivalent cationic salts are expected to act as dynamic noncovalent crosslinkers by linking together two or more Nafion sulfonate groups. In order to test the effect that these ionic crosslinkers had on TTF, Nafion films were immersed in 1M solutions of $CaCl_2$, $FeCl_2$, $MgCl_2$, $ZnCl_2$, or $Ba(OAc)_2$ for 10 minutes the dried at RT or 90 °C. Films immersed in $Ba(OAc)_2$ solutions showed significant buckling/warping during the drying process and peeled off of the glass substrate; therefore $Ba(OAc)_2$ was not examined further as a crosslinker. TTF Results are summarized in Figure 10.

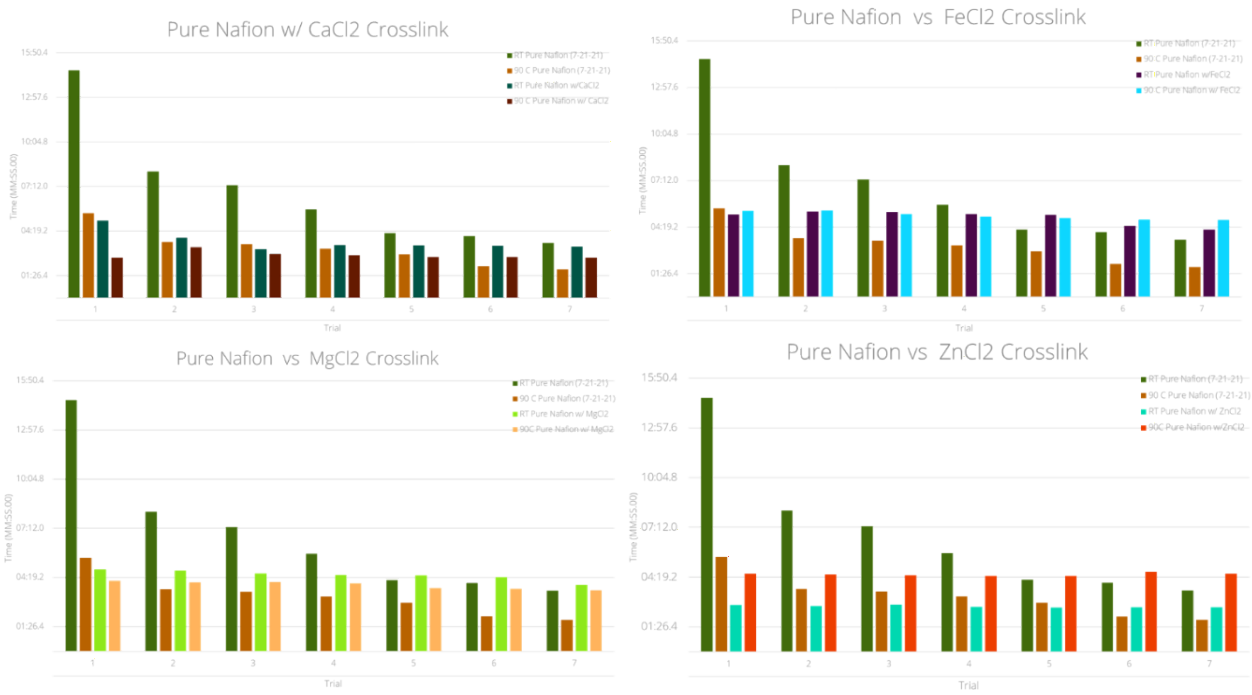

Figure 10. TTF for Nafion films dried at RT or 90 °C and crosslinked with various multivalent salts at 1-7 freeze/thaw cycles.

Initially, the inclusion of cationic crosslinker decreased the TTF for all films during the first few trials compared to neat Nafion dried at RT By the 7th freeze/thaw however all crosslinked films out-performed or matched neat Nafion films with the exception of $ZnCl_2$ and $CaCl_2$ crosslinked films dried at RT which matched of frosted slightly quicker that neat Nafion films also dried at RT. These results suggest that crosslinking might improve the stability of TTF over multiple freeze/thaw cycles but at the cost of quicker initial TTF. Nafion films blended with the most promising antifreezing agents (PEG and PEG-Me) were also crosslinked and screened, where the most promising results were achieved using $CaCl_2$ and are summarized in Figure 11.

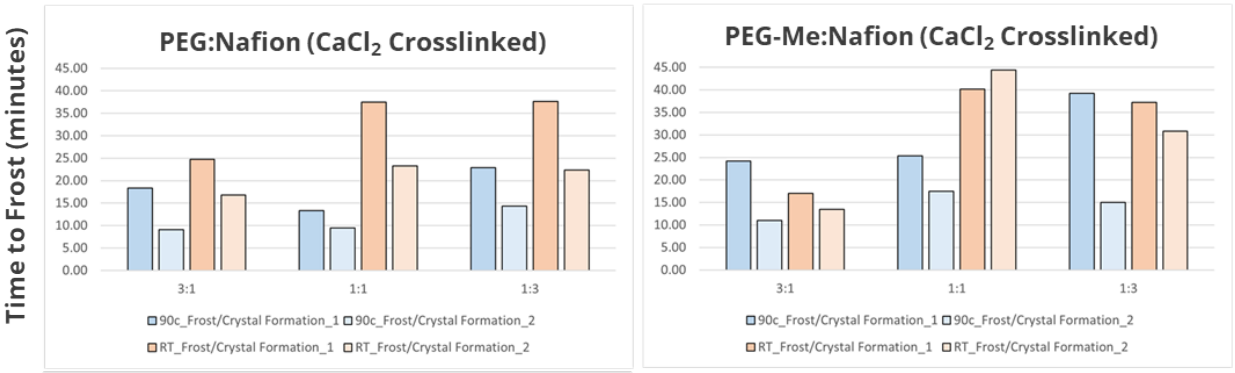

Figure 11. TTF for Nafion/PEG and Nafion/PEG-Me blended films reported as ratio by vol. of PEG/PEG-ME solution (20 wt.%) to Nafion (5 wt.%) used for dip-coating solutions. 1 and 2 refer to the first and second freeze/thaw cycle respectively. Films were crosslinked by soaking in a 1M aqueous solution of $CaCl_2$ for 10 minutes then left to dry under ambient conditions.

The highest performing PEG or PEG-Me and Nafion blended films (1:3) had a TTF of ~27 and ~24 minutes respectively on the first trial. Crosslinking these films with $CaCl_2$ improved this even further to ~36 minutes for 1:1 and 1:3 PEG:Nafion blended films dried at RT and ~36-40 minutes for 1:1 and 1:3

PEG:Nafion blended films (Figure 11). Perhaps the most promising result was that the reduction in TTF for $CaCl_2$ crosslinked PEG-Me/Nafion films between trials 1 and 2 was the lowest of any observed previously; in fact TTF increased slightly for the 1:1 blended film. Eventually similar cracking/fracturing was observed in all films at later trials. Therefore the same two antifreezing agents and $CaCl_2$ crosslinker were explored using dip-coated films prepared from a higher concentration Nafion dispersion (20 wt.% instead of 5 wt.%) in the hopes of coating thicker more robust films.

3.5. Thicker Films

Dip-coated blended PEG/PEG-Me and Nafion films were prepared identically to those previously examined with two exceptions; first the concentration of the Nafion dispersion used for dip-coating was increased to 20 wt.% from 5 wt.% to increase the viscosity and thickness of dip-coated films. This was confirmed using profilometry which showed an increase in films thicknesses to a typical range of 20-30 µm from 3-14 µm (Figure 12). Second, $CaCl_2$ was added directly to dip-coating solutions at a 1:10 $CaCl_2$:Nafion ratio (by weight) instead of soaking films in a 1M $CaCl_2$ solution. This was done to ensure that crosslinker was present throughout the film and not confined to the surface.

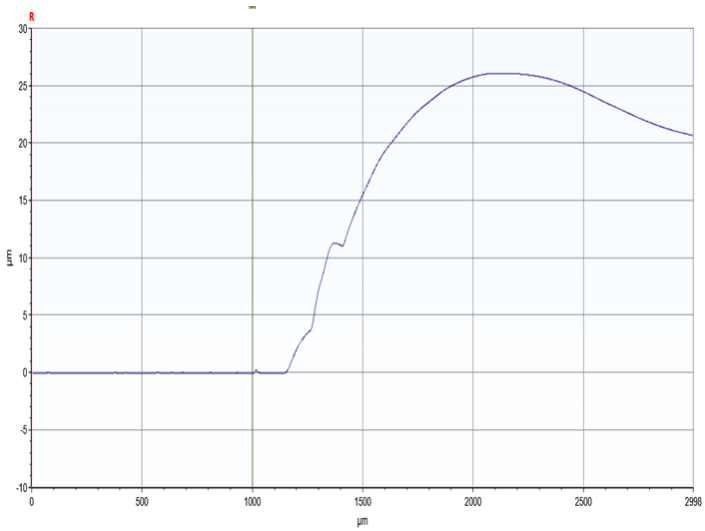

Figure 12. Profilometry of 1:5.5 PEG-Me:Nafion blended film by vol. of PEG/PEG-ME solution (20 wt.%) to Nafion (20 wt.%) used for dip-coating solutions and dried at RT.

Figure 13. TTF for Nafion/PEG and Nafion/PEG-Me blended films reported as ratio by vol. of PEG/PEG-ME solution (20 wt.%) to Nafion (20 wt.%) used for dip-coating solutions. 1 and 2 refer to the first and second freeze/thaw cycle respectively. Asterix denotes that frost formation equivalent to previous results was observed to form on the film surface. Non-asterix marked results indicate the time at which individual ice crystals were observed on the film surface, but no frost-over phenomena was seen during the time over which the experiment was held at -25°C

The results achieved in these blended films, both crosslinked and un-crosslinked, were by far the most promising out of any previously collected. In fact TTFs were so greatly increased that in many cases experiments were terminated as no frost was observed during the time over which the experiment was held at -25 °C (upwards of an hour in some cases). In these situations, the time was marked as the time at which individual ice crystals were observed as starting to form on the film surface (Figure 13).

In order to probe what the highest time to frostover/hazing the blended films could achieve, the crosslinked and un-crosslinked films with the highest times to ice crystal formation (1:5.5 PEG:Nafion dried at RT and 1:2 PEG-Me:Nafion with $CaCl_2$ dried at 90 °C were re-tested at -25 °C for an extended period of time (Figure 14). At 18 minutes both films remain transparent and unfrosted compared to uncoated portions of the glass slide which has frosted over. At 1 hour 18 minutes ice crystals have formed on the surface of both films (to a greater extent on the crosslinked film) but the films remain transparent and unfrosted. At 3 hours 5 minutes ice crystals have obscured the crosslinked film and begun to accumulate further on the uncrosslinked PEG/Nafion film, however the uncrosslinked film remains transparent and unfrosted. At this point the experiment was terminated, however in both cases the results demonstrate a dramatic improvement over the performance of both untreated glass and neat dip-coated Nafion films dried at RT or 90 °C

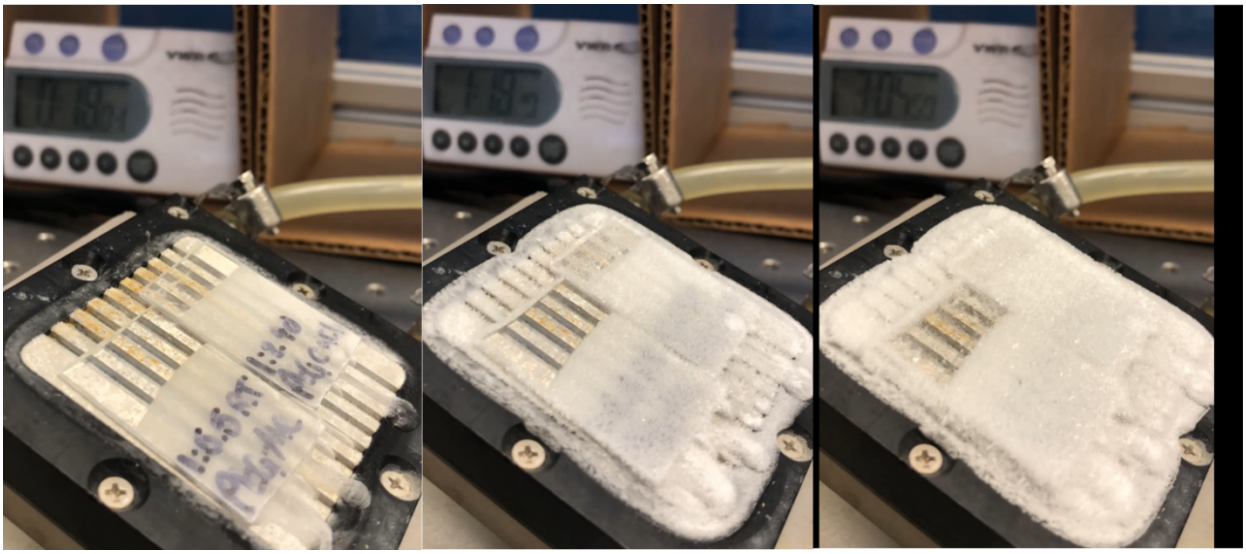

Figure 14. Ice formation on 1:5.5 PEG:Nafion blended film dried at RT (left-most slide) and 1:2 PEG-Me:Nafion blended film crosslinked with $CaCl_2$ dried at 90 °C (right-most slide) dip-coated on glass and held at -25 °C on Peltier plate. Stopwatch in background displays elapsed time (h:mm:ss).

4. NUMERICAL SIMULATIONS OF ION COMPLEXATION IN POLYACRYLIC ACID/WATER

4.1. Model and Methodology

Two sets of simulations were carried out to explore the effect of varying counterions on the properties of fully deprotonated polyacrylic acid (PAA) in the presence of water. In the first set, PAA/water systems with varying fractions of water were modeled with 4 different counterions, two monovalent counterions (K^+ and Na^+) and two divalent counterions (Ca^{2+} and Mg^{2+}). The wt% of PAA in these systems was varied from ~10 to 80 wt% PAA for temperatures from 250K to 400K. In the second set of simulations, the interpenetration of water into a dry PAA film was studied for Na^+ or Ca^{2+} counterions for temperatures between 300K and 400K.

All the PAA system was built using the CHARMM-GUI polymer builder.[70, 71] For the PAA/water solutions, the initial systems was built with 20 atactic PPA chains of length n = 50 monomers and 17, 176 water molecules as illustrated in Figure 1. The weight fraction of PAA in this initial system is ~10 wt%. Systems with higher weight fraction of PPA chains were made by removing a designated fraction of the water molecules and re-equilibrating at constant pressure of P = 1 bar. The initial PAA/water system was built with K^+ counterions. For the divalent counterion systems, half the counterions were deleted and the charge increased to 2+. All systems are periodic in all three directions. For the interpenetration studies, the initial system consisted of 10 distinct atactic PAA polymers of length *n* = 50 monomers, each of which is replicated 20 times and neutralized with either Na^+ or Ca^{2+} counterions. As described below, after the dry PAA systems was equilibrated, the chains were unfolded in the z-direction to produce a membrane. A water film was added on top of the membrane and the interpenetration of water into the film was followed as a function of time.

The intermolecular forces were described by Lennard-Jones interactions with attractive r−6 and repulsive r−12 terms and long-range Coulomb interactions. The van der Waals forces were truncated at 1.2 nm with a smoothing function starting at 1.0 nm, reaching zero at the cutoff. The PAA/water simulations were carried out using the LAMMPS MD simulation package[72] with a time step of 2 f. All electrostatic interactions closer than 1.2 nm are calculated in real space, and those beyond this range are calculated in reciprocal Fourier space by using the particle−particle particle-mesh algorithm (PPPM)[73] with a precision of 10−6. Temperature is maintained using a Nose-Hoover thermostat[74, 75] with a time constant of 100 fs. All bonded and non-bonded polymer and ion interactions are obtained from the CHARMM-GUI server.[70, 71] Water was modeled with the TIP4P/Ice water model.[76, 77] The interpenetration simulations were carried out using the GROMACS 2021 simulation suite.[78] In this case, the long-range electrostatic interactions were treated using the potential-mesh Ewald (PME) method,[79, 80] with a Fourier grid spacing of 0.12 nm. The real-space cutoff is tuned at run time to optimize performance. The bond length of all bonds involving hydrogen atoms is constrained using the PLINCS algorithm,[81] with a time step of 2 fs for temperatures T < 400K and 1 fs for T = 400K. Temperature is maintained using the Bussi et al.[82] stochastic rescaling thermostat and a time constant of 100 fs. Analysis of xtc files is handled using the MDAnalysis python package.[83]

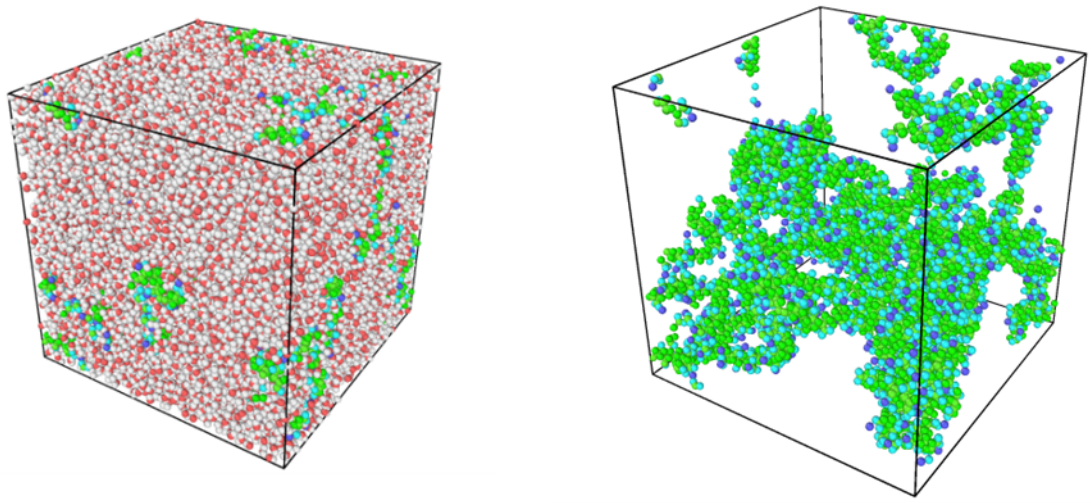

Figure 15. 20 deprotonated PAA chains of n = 50 monomers in water, ~ 10 wt % PAA. PAA molecules are green, Ca^{2+} counterions are blue, O in water is red and H in water is white. Images made using Ovito.[84]

4.2. Water/Ion Transport in PAA/Water Solutions

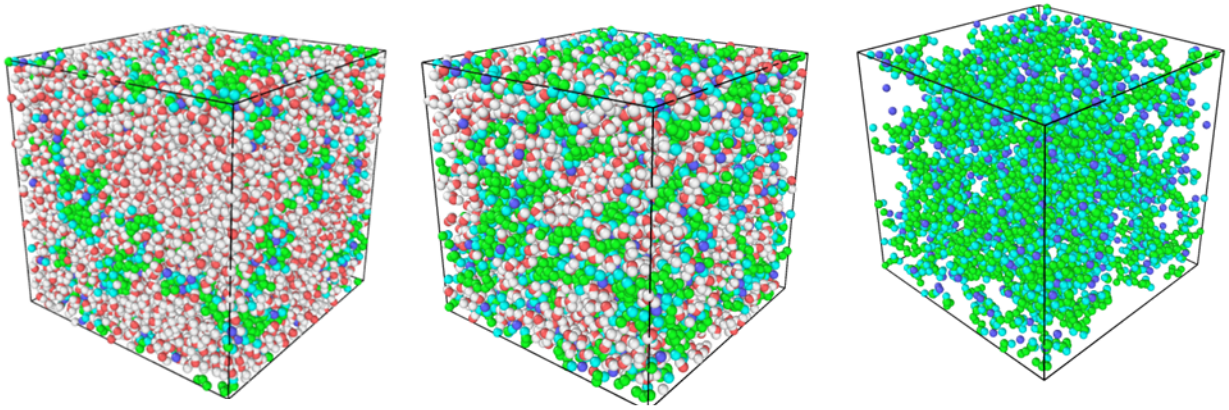

Figure 16. Illustration of PAA/water system at ~18 wt% PAA (left) and ~47 wt% PAA (middle). Right image shows the ~47 wt% PAA system with water removed. Colors are same as in Figure 15. 20 deprotonated PAA chains of n = 50 monomers in water, ~ 10 wt % PAA. PAA molecules are green, Ca^{2+} counterions are blue, O in water is red and H in water is white. Images made using Ovito.[84]

The mobility of water and the counterions were studied as a function of temperature and water fraction. Figure 16 shows examples of the system at different weight fractions of PAA. Differences in the properties of the counterions can be seen in Figure 17a, where the fraction f_c of condensed counterions is plotted as a function of weight fraction of PAA. All of Ca^{2+} counterions are condensed (with 3.5 Å) of at

least one PAA oxygen for all water fractions. This is in contrast with the condensed fraction of K^+ and Mg^{2+}, which increases with decreasing water content.

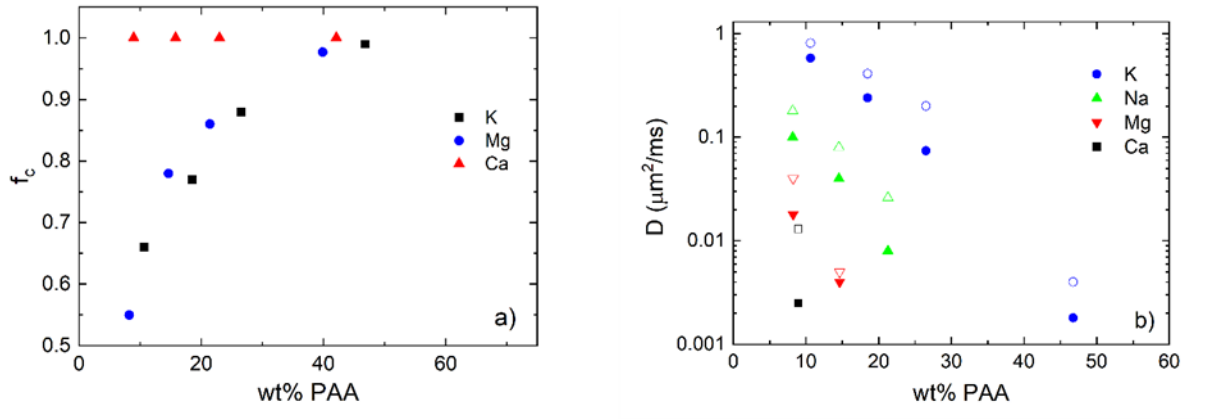

Figure 17. a) Fraction of counterions condensed (with 3.5 Å) of PAA oxygen at 300 K as a fraction of PAA weight fraction for 3 counterions. b) Diffusion of counterions at 300 K (solid) and 350 K (open) as function of PAA weight fraction.

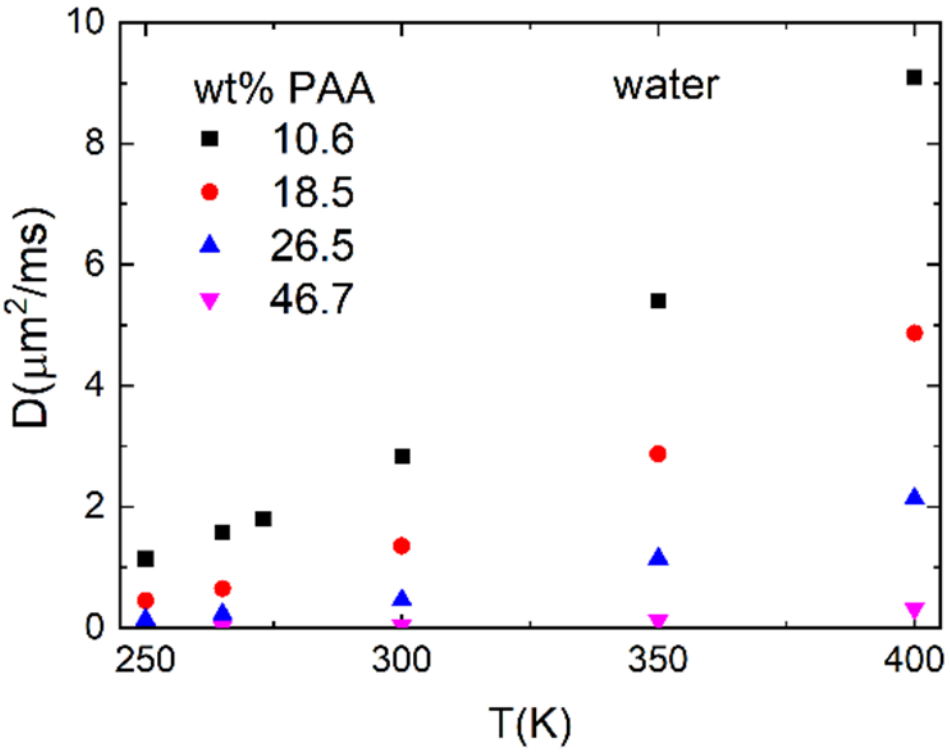

Figure 18. Temperature dependence of the water diffusion for 4 values of the weight fraction of PAA.

This difference directly effects the counterion diffusion, which is shown in Figure 17b. The two monovalent counterions (K^+ and Na^+) are significantly more mobile than the two divalent counterions (Ca^{2+} and Mg^{2+}). The fact that all the Ca^{2+} counterions are condensed, even at very high-water concentration, leads to a significantly lower diffusion for Ca^{2+}. Remarkedly, the diffusion constant of Ca^{2+} being more than two orders of magnitude lower than K^+.

The diffusion of water does not depend on the counterion. Figure 18 shows temperature dependence of the water diffusion for 4 values of the weight fraction of PAA. For lower water fractions, the diffusion was too small to accurately measure. Note that even well below the freezing temperature of water, the water molecules were mobile and did not freeze over the course of the simulations (several hundred nanoseconds).

4.3. Water Interpenetration into PAA films

For the interpenetration studies, four dry PAA systems at different densities were created using different annealing procedures. The two systems with different counterions were first equilibrated for 1 ns at constant pressure P = 1 bar and T = 300 K and 1 bar. Pressure is maintained using the Berendsen et al. barostat[85] with a time constant of 1 ps and compressibility of 4.5×10^{-5} (1/bar). A 10 ns equilibration run was then conducted with a Nose-Hoover thermostat with a time constant of 0.5 ps and a Parrinello-Raman barostat.[74, 75, 86] Several different systems were created using different annealing conditions. In the first system, no further annealing was conducted. In the second, equilibration was conducted by initializing the temperature at 600 K and reducing the T to 300 K over 500 ns and then running at 300 K for 500 ns, all at 1 bar. In the third, the same procedure was used but with a higher initial temperature of 1000 K. Finally, a more complex annealing procedure developed by Abbott and Frischknecht[87] was used, which leads to higher densities. This method first involves compressing the system at 100 bar and 600 K to a density of 0.7 g/cm^{-3}. The simulation is then run at constant volume and 1000 K for 600 ps. Next, a series of nine sets of three types of runs is conducted: a 50 ps NVT simulation at 1000 K, a 100 ps NVT simulation at 313 K, and a 50 ps NPT simulation at 313 K and a different pressure for each of the nine runs: 1000, 10000, 5000, 1000, 500, 100, 10, and 1 bar. For this step, then, the system undergoes NVT at high temperature, NVT at low temperature, NPT at P1, NVT at high temperature, NVT at low temperature, NPT at P2, etc. The final NPT run is conducted for a duration of 2 ns. After this, there is a final series of 14 NVT runs: 1 ns at 2000 K and then 100 ps at each of 1800, 1600, 1400, 1200, 1000, 900, 800, 700, 600, 500, 400, and 313 K, successively. The final density of PAA systems in each case are shown in Table I .

Table 2. Density at T = 300K and different annealing conditions for Na^+ and Ca^{2+} counterions.

Annealing	Density (kg/m^3), Na^+	Density (kg/m^3), Ca^{2+}
None	1464	1353
600 K	1659	1473
1000 K	1722	1569
Custom	1747	1580

After equilibration, the PAA chains were unwrapped in the z-direction and placed in a larger simulation cell with repulsive wall in the xy plane at the top, 10 nm above the top surface. The system remained periodic in the x and y directions. After a short equilibration to allow the unfolded chains to relax, the system was solvated with a 6 nm thick water film above the polymer as shown in Figure 19a, leaving a 4 nm gap at the top to allow the vapor pressure of the water to maintain the pressure of the system. Water was modeled with the TIP4P/Ice water model.[76, 77] This system is then equilibrated using steepest-descent energy minimization and then a 2 ns NVT run at 300 K with polymer atoms restrained.

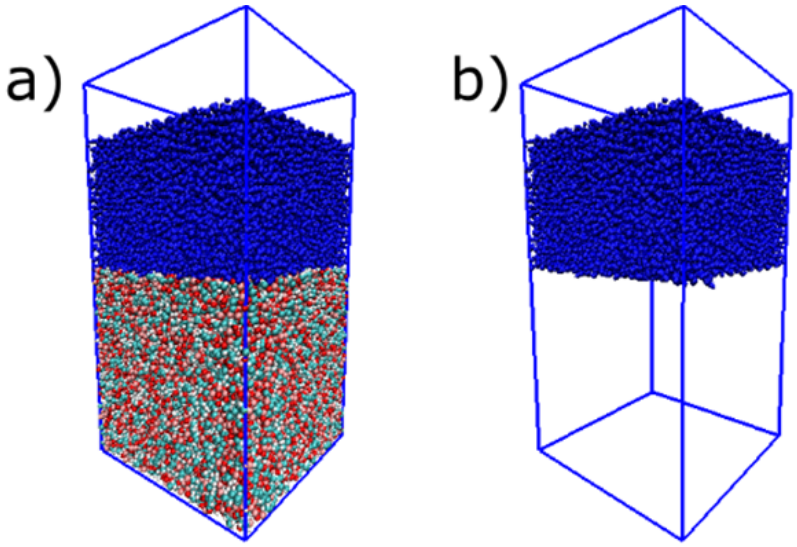

Figure 19. Initial conditions for highest density system with Na+ counterions. All atoms are shown in (a) and only water molecules are shown in (b). All water molecules are blue, carbon atoms are teal, oxygen atoms in polymers are red, hydrogen atoms in polymers are white, and ions are pink. Images made using VMD.[1]

Figure 19 shows images of the initial conditions of the highest density systems. After solvation and equilibration, each system is simulated for at least 1.0 μs. The density of polymer and water for each system at various times is shown in Figure 20 for the second PPA system (annealed at 600K). Profiles for the other systems are similar, though the systems that are intensely annealed (higher density) exhibit noticeably less water penetration into the membrane than the systems with less annealing. As expected, the uptake is higher at higher temperatures. In each case, systems containing Ca^{2+} counterions allow water more readily into the membrane than those with Na^{+} counterions. From these systems, the 1000 K annealed systems and the unannealed systems were selected for further simulation and analysis. Runs in these cases for each counterion at T = 300, 350 and 400 K are extended to greater durations

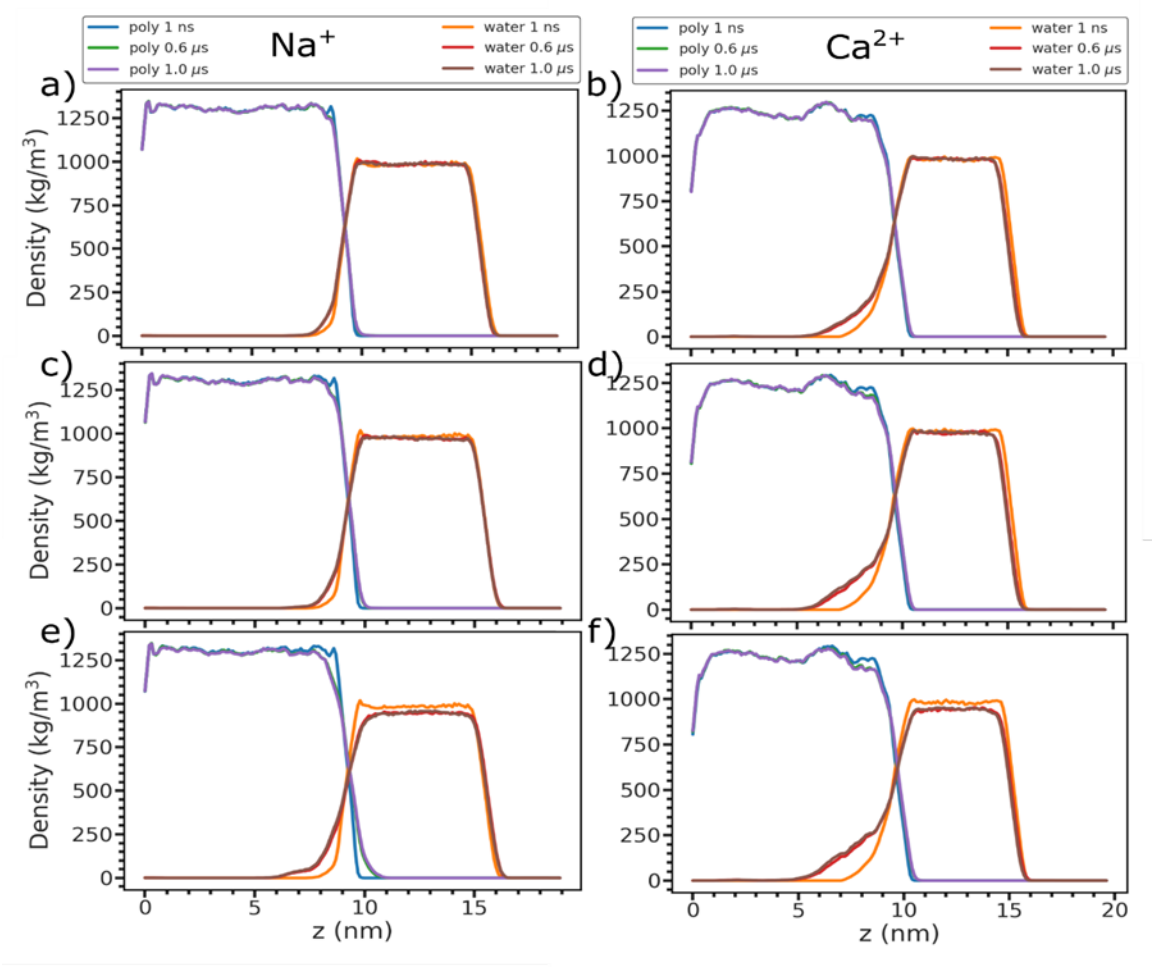

Figure 20. Densities of membrane systems as a function of distance perpendicular to the membrane for the membrane annealed at 600 K for polymer and water atoms at different times. a, c, e for Na^+ ions and b, d, f for Ca^{2+} ions. a and b for 300 K, c and d for 350 K, e and f for 400 K

The water uptake in each of these systems is quantified by measuring the total mass of water in the membrane as a function of time. We identify water in the membrane by using the point at which the density of water is less than the density of polymer. Water update as a function of time is shown in Figure 21. As seen from these results the density of the PAA film has a significant effect on the amount of water uptake.

.

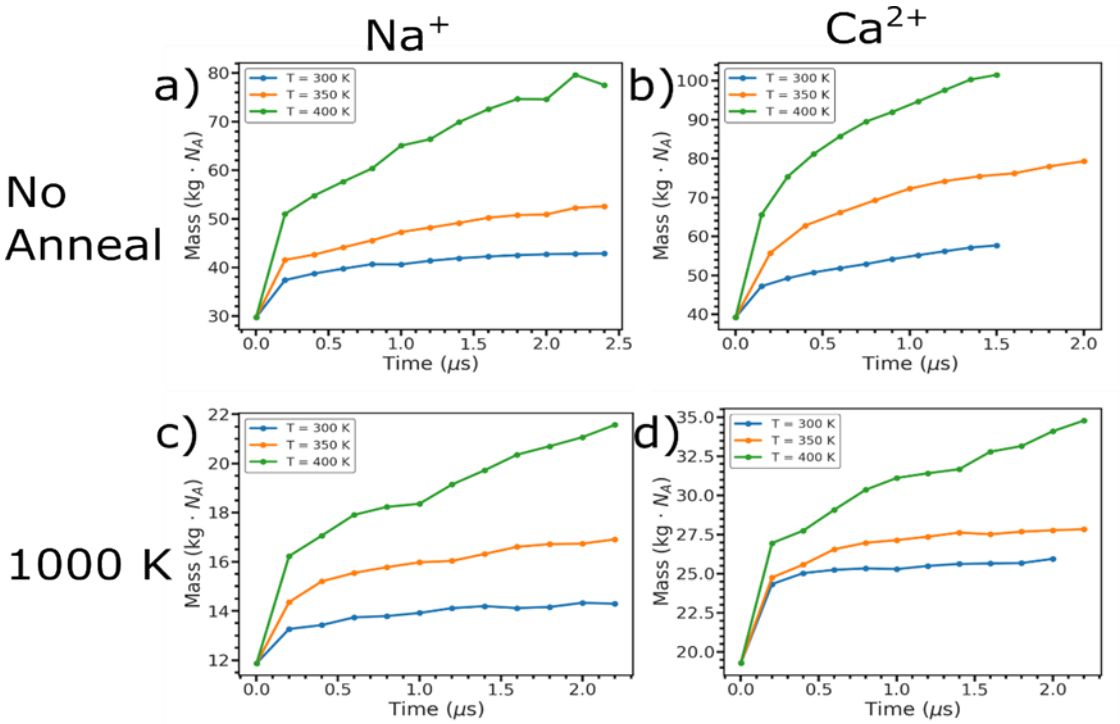

Figure 21. Mass of water contained in the membrane as a function of simulation time (scaled by Avogadro´s number) for Na^+ ions (a,c) and Ca^{2+} ions (b,d) for PAA systems that underwent no annealing (a,b) and 1000 K annealing (c,d).

From the simulations, one can follow the path of individual water molecules as they infiltrate the membrane. This is illustrated in Figure 22. In a), the water molecule, located in the center of the figure, is hydrogen bonded with two adjacent PAA oxygen atoms. In b), one of the COO^- residues rotates away from the water molecule. In c), the water molecule swings around to the other side of the other COO^- oxygen. Finally, the water dissociates from the last oxygen atom and continues further into the membrane.

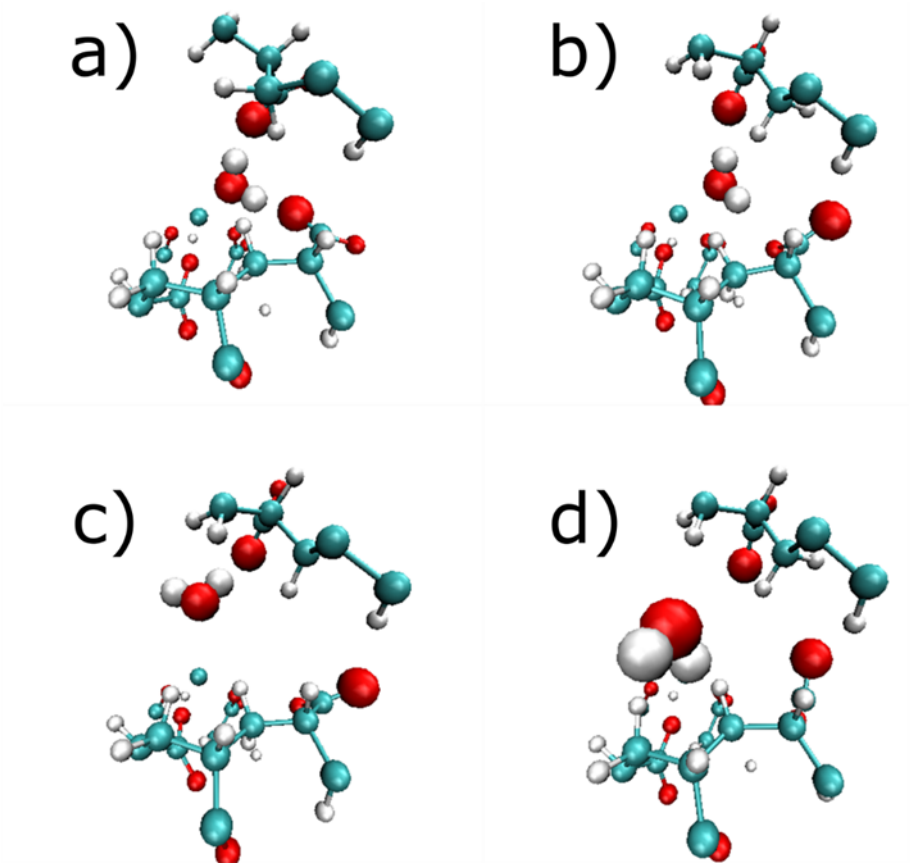

Figure 22. Path of a water molecule as it travels through the membrane. Oxygen atoms are red, hydrogen atoms are white, and carbon atoms are silver.

REFERENCES

1. Humphrey, W., A. Dalke, and K. Schulten, VMD: visual molecular dynamics. J. Mol. Graphics, 1996. 14: p. 33-38.
2. Azimi Dijvejin, Z., et al., Smart low interfacial toughness coatings for on-demand de-icing without melting. Nat Commun, 2022. 13(1): p. 5119.
3. Irajizad, P., S. Nazifi, and H. Ghasemi, Icephobic surfaces: Definition and figures of merit. Adv Colloid Interface Sci, 2019. 269: p. 203-218.
4. Kreder, M.J., et al., Design of anti-icing surfaces: smooth, textured or slippery? Nature Reviews Materials, 2016. 1(1).
5. Lin, Y., et al., Recent Progress in Preparation and Anti-Icing Applications of Superhydrophobic Coatings. Coatings, 2018. 8(6): p. 208.
6. Huang, X., et al., A survey of icephobic coatings and their potential use in a hybrid coating/active ice protection system for aerospace applications. Progress in Aerospace Sciences, 2019. 105: p. 74-97.
7. Esmeryan, K.D., From Extremely Water-Repellent Coatings to Passive Icing Protection—Principles, Limitations and Innovative Application Aspects. Coatings, 2020. 10(1): p. 66.
8. Hakimian, A., S. Nazifi, and H. Ghasemi, Metrology of Ice Adhesion, in Ice Adhesion. 2020. p. 217-236.
9. Rønneberg, S., et al., Interlaboratory Study of Ice Adhesion Using Different Techniques. Coatings, 2019. 9(10): p. 678.
10. Zhang, Z.S. and X.Y. Liu, Control of ice nucleation: freezing and antifreeze strategies. Chemical Society Reviews, 2018. 47(18): p. 7116-7139.
11. Zhang, Z., et al., An experimental study on the detrimental effects of deicing fluids on the performance of icephobic coatings for aircraft icing mitigation. Aerospace Science and Technology, 2021. 119.
12. Kim, P., et al., Liquid-Infused Nanostructured Surfaces with Extreme Anti-Ice and Anti-Frost Performance. Acs Nano, 2012. 6(8): p. 6569-6577.
13. Wilson, P.W., et al., Inhibition of ice nucleation by slippery liquid-infused porous surfaces (SLIPS). Physical Chemistry Chemical Physics, 2013. 15(2): p. 581-585.
14. Biggs, C.I., et al., Polymer mimics of biomacromolecular antifreezes. Nat Commun, 2017. 8(1): p. 1546.
15. Gwak, Y., et al., Creating Anti-icing Surfaces via the Direct Immobilization of Antifreeze Proteins on Aluminum. Sci Rep, 2015. 5: p. 12019.
16. Lv, J.Y., et al., Bio-Inspired Strategies for Anti-Icing. Acs Nano, 2014. 8(4): p. 3152-3169.
17. Wang, S., et al., Icephobicity of Penguins Spheniscus Humboldti and an Artificial Replica of Penguin Feather with Air-Infused Hierarchical Rough Structures. The Journal of Physical Chemistry C, 2016. 120(29): p. 15923-15929.
18. Xu, Y., et al., Anti-Freezing multiphase gel materials: Bioinspired design strategies and applications. Giant, 2020. 2.
19. Inagawa, A., N. Uehara, and T. Okada, Interaction between antifreeze protein and ice crystal facet evaluated by ice-channel electrophoretic measurements of threshold electric field strength. Anal Chim Acta, 2020. 1110: p. 122-130.
20. Clark, J.K., 2nd, S.J. Paddison, and S.J. Hamrock, The effect of hydrogen bond reorganization and equivalent weight on proton transfer in 3M perfluorosulfonic acid ionomers. Phys Chem Chem Phys, 2012. 14(47): p. 16349-59.

21. Bahadur, V., et al., Predictive Model for Ice Formation on Superhydrophobic Surfaces. Langmuir, 2011. 27(23): p. 14143-14150.
22. Dou, R.M., et al., Anti-icing Coating with an Aqueous Lubricating Layer. Acs Applied Materials & Interfaces, 2014. 6(10): p. 6998-7003.
23. Makki, H., H. Yahyaei, and M. Mohseni, Superhydrophobic antiicing and ice-release polymer coatings. 2019: p. 205-222.
24. Cao, L.L., et al., Anti-Icing Superhydrophobic Coatings. Langmuir, 2009. 25(21): p. 12444-12448.
25. Egorkin, V.S., et al., Icephobic Performance of Combined Fluorine-Containing Composite Layers on Al-Mg-Mn-Si Alloy Surface. Polymers (Basel), 2021. 13(21).
26. Wu, X., et al., When superhydrophobic coatings are icephobic: Role of surface topology. Surface and Coatings Technology, 2019. 358: p. 207-214.
27. Chen, X., L. Hu, and Y. Du, Anti-icing and anti-frost properties of structured superhydrophobic coatings based on aluminum honeycombs. Materials Chemistry and Physics, 2022. 291.
28. Heale, F.L., I.P. Parkin, and C.J. Carmalt, Slippery Liquid Infused Porous TiO2/SnO2 Nanocomposite Thin Films via Aerosol Assisted Chemical Vapor Deposition with Anti-Icing and Fog Retardant Properties. ACS Appl Mater Interfaces, 2019. 11(44): p. 41804-41812.
29. Epstein, A.K., et al., Liquid-infused structured surfaces with exceptional anti-biofouling performance. Proceedings of the National Academy of Sciences of the United States of America, 2012. 109(33): p. 13182-13187.
30. Chen, J., et al., Durable Anti-Icing Coatings Based on Self-Sustainable Lubricating Layer. ACS Omega, 2017. 2(5): p. 2047-2054.
31. Chen, J., et al., Robust Prototypical Anti-icing Coatings with a Self-lubricating Liquid Water Layer between Ice and Substrate. Acs Applied Materials & Interfaces, 2013. 5(10): p. 4026-4030.
32. Golovin, K., et al., Designing Durable Icephobic Surfaces. Sci. Adv., 2016. 2: p. e1501496.
33. He, Z., et al., Bioinspired Multifunctional Anti-icing Hydrogel. Matter, 2020. 2(3): p. 723-734.
34. Li, Y., et al., Highly Transparent and Water-Enabled Healable Antifogging and Frost-Resisting Films Based on Poly(vinyl alcohol)–Nafion Complexes. Chemistry of Materials, 2016. 28(19): p. 6975-6984.
35. Chen, P., et al., An extreme environment-tolerant anti-icing coating. Chemical Engineering Science, 2022. 262.
36. Cui, J., et al., Dynamic polymer systems with self-regulated secretion for the control of surface properties and material healing. Nature Materials, 2015. 14(8): p. 790-795.
37. Li, R.a., et al., Autonomous Self-Healing, Antifreezing, and Transparent Conductive Elastomers. Chemistry of Materials, 2020. 32(2): p. 874-881.
38. Kim, P., et al., Hydrogel-actuated integrated responsive systems (HAIRS): Moving towards adaptive materials. Current Opinion in Solid State & Materials Science, 2011. 15(6): p. 236-245.
39. Oh, J.Y., et al., Intrinsically stretchable and healable semiconducting polymer for organic transistors. Nature, 2016. 539(7629): p. 411-415.
40. Biggs, C.I., et al., Polymer mimics of biomacromolecular antifreezes. Nature Communications, 2017. 8.
41. Ma, D., et al., Hyperbranched Polyglycerol as a Colloid in Cold Organ Preservation Solutions. Plos One, 2015. 10(2): p. e0116595.
42. Tao, C., et al., Formation of zwitterionic coatings with an aqueous lubricating layer for antifogging/anti-icing applications. Progress in Organic Coatings, 2018. 115: p. 56-64.

43. Koivuluoto, H., et al., Anti-icing Behavior of Thermally Sprayed Polymer Coatings. Journal of Thermal Spray Technology, 2016. 26(1-2): p. 150-160.
44. Yu, Y., et al., A promising self-assembly PTFE coating for effective large-scale deicing. Progress in Organic Coatings, 2020. 147.
45. Mauritz, K.A. and R.B. Moore, State of understanding of Nafion. Chemical Reviews, 2004. 104(10): p. 4535-4585.
46. Gardiner, J., Fluoropolymers: Origin, Production, and Industrial and Commercial Applications. Australian Journal of Chemistry, 2015. 68(1).
47. Mauritz, K.A. and R.B. Moore, State of understanding of nafion. Chem Rev, 2004. 104(10): p. 4535-85.
48. Mendil-Jakani, H., et al., Water crystallization inside fuel cell membranes probed by X-ray scattering. Journal of Membrane Science, 2011. 369(1-2): p. 148-154.
49. Teocoli, F., et al., Effects of water freezing on the mechanical properties of nafion membranes. Journal of Polymer Science Part B: Polymer Physics, 2012. 50(20): p. 1421-1425.
50. Plazanet, M., et al., Water in a polymeric electrolyte membrane: Sorption/desorption and freezing phenomena. Journal of Membrane Science, 2014. 453: p. 419-424.
51. Ma, Z.R., et al., NMR studies of proton transport in fuel cell membranes at sub-freezing conditions. Journal of Materials Chemistry, 2011. 21(25): p. 9302-9311.
52. Alvarez-Gallego, Y. and M.P. de Heer, Sub-Freezing Conductivity of PFSA Membranes. Fuel Cells, 2009. 9(4): p. 421-431.
53. Kusoglu, A. and A.Z. Weber, New Insights into Perfluorinated Sulfonic-Acid Ionomers. Chemical Reviews, 2017. 117(3): p. 987-1104.
54. Goswami, S., S. Klaus, and J. Benziger, Wetting and absorption of water drops on nafion films. Langmuir, 2008. 24(16): p. 8627-8633.
55. Marcus, Y., Effect of Ions on the Structure of Water: Structure Making and Breaking. Chemical Reviews, 2009. 109: p. 1346-1370.
56. Bass, M., et al., Surface Structure of Nafion in Vapor and Liquid. J. Phys. Chem. B 2010, 114, , 2010. 114: p. 3784–3790.
57. Dura, J.A., et al., Multilamellar Interface Structures in Nafion. Macromolecules, 2009. 42(13): p. 4769-4774.
58. Allen, F.I., et al., Morphology of Hydrated As-Cast Nafion Revealed through Cryo Electron Tomography. ACS Macro Lett, 2015. 4(1): p. 1-5.
59. Zakharova, J.A., et al., Controlled modification of Nafion membrane with cationic surfactant. Colloid and Polymer Science, 2018. 296(5): p. 835-846.
60. Kelarakis, A. and E.P. Giannelis, Nafion as cosurfactant: solubilization of nafion in water in the presence of Pluronics. Langmuir, 2011. 27(2): p. 554-60.
61. Gasa, J.V., R.A. Weiss, and M.T. Shaw, Ionic crosslinking of ionomer polymer electrolyte membranes using barium cations. Journal of Membrane Science, 2007. 304(1-2): p. 173-180.
62. Yang, F., et al., Investigation of the Interaction between Nafion Ionomer and Surface Functionalized Carbon Black Using Both Ultrasmall Angle X-ray Scattering and Cryo-TEM. ACS Appl Mater Interfaces, 2017. 9(7): p. 6530-6538.
63. Rubatat, L., et al., Evidence of Elongated Polymeric Aggregates in Nafion. Macromolecules, 2002. 35(10): p. 4050-4055.
64. Cirkel, P.A., T. Okada, and S. Kinugasa, Equilibrium Aggregation in Perfluorinated Ionomer Solutions. Macromolecules, 1998. 32(2): p. 531-533.
65. Bunkin, N.F., et al., Study of the Phase States of Water Close to Nafion Interface. WATER journal, 2013. 4.

66. Bunkin, N.F., et al., Colloidal crystal formation at the "Nafion-water" interface. J Phys Chem B, 2014. 118(12): p. 3372-7.
67. Schlick, S., et al., Fluorine-19 NMR spectroscopy of acid Nafion membranes and solutions. Macromolecules, 2002. 24(12): p. 3517-3521.
68. Lamch, L., et al., Hydrophobically Functionalized Poly(Acrylic Acid) Comprising the Ester-Type Labile Spacer: Synthesis and Self-Organization in Water. Polymers (Basel), 2020. 12(5).
69. Bell, N.S., et al., Polymer intercalation synthesis of glycoboehmite nanosheets. Applied Clay Science, 2021. 214.
70. Jo, S., et al., CHARMM-GUI: a web-based graphical user interface for CHARMM. J. Comp. Chem., 2008. 29: p. 1859-1865.
71. Choi, Y.K., et al., CHARMM-GUI polymer builder for modeling and simulation of synthetic polymers. J. Chem. Theory Comp., 2021. 17: p. 2431-2443.
72. Thompson, A.P., et al., LAMMPS-a flexible simulation tool for particle-based materials modeling at the atomic, meso, and continuum scales. Comp. Phys. Comm., 2022. 271: p. 108171.
73. Hockney, R.W. and J.W. Eastwood, Computer simulation using particles. 2021: crc Press.
74. Nosé, S., A molecular dynamics method for simulations in the canonical ensemble. Mol. Phys., 1984. 52: p. 255-268.
75. Hoover, W.G., Canonical dynamics: Equilibrium phase-space distributions. Phys. Rev. A, 1985. 31: p. 1695.
76. Abascal, J., et al., A potential model for the study of ices and amorphous water: TIP4P/Ice. J. Chem. Phys., 2005. 122: p. 234511.
77. Vega, C., J. Abascal, and I. Nezbeda, Vapor-liquid equilibria from the triple point up to the critical point for the new generation of TIP4P-like models: TIP4P/Ew, TIP4P/2005, and TIP4P/ice. J. Chem. Phys., 2006. 125: p. 034503.
78. Brooks, B.R., et al., CHARMM: the biomolecular simulation program. J. Comp. Chem., 2009. 30: p. 1545-1614.
79. Darden, T., D. York, and L. Pedersen, Particle mesh Ewald: An N· log (N) method for Ewald sums in large systems. J. Chem. Phys., 1993. 98: p. 10089-10092.
80. Essmann, U., et al., A smooth particle mesh Ewald method. J. Chem. Phys., 1995. 103: p. 8577-8593.
81. Hess, B., P-LINCS: A parallel linear constraint solver for molecular simulation. J. Chem. Theory Comp., 2008. 4: p. 116-122.
82. Bussi, G., D. Donadio, and M. Parrinello, Canonical sampling through velocity rescaling. J. Chem. Phys., 2007. 126: p. 014101.
83. Gowers, R.J., et al. MDAnalysis: a Python package for the rapid analysis of molecular dynamics simulations. in Proceedings of the 15th python in science conference. 2016. SciPy Austin, TX.
84. Stukowski, A., Visualization and analysis of atomistic simulation data with OVITO–the Open Visualization Tool. Model. Sim. Materials Sci, Eng., 2009. 18: p. 015012.
85. Berendsen, H.J., et al., Molecular dynamics with coupling to an external bath. J. Chem. Phys., 1984. 81: p. 3684-3690.
86. Parrinello, M. and A. Rahman, Polymorphic transitions in single crystals: A new molecular dynamics method. J. Appl. Phys., 1981. 52: p. 7182-7190.
87. Abbott, L.J. and A.L. Frischknecht, Nanoscale structure and morphology of sulfonated polyphenylenes via atomistic simulations. Macromolecules, 2017. 50: p. 1184-1192.

APPENDIX A. ANTI-FREEZING PATENT HISTORY

Patent No.	Year Filed	Year Granted	Assignee	Abstract
9945247	2015	2018	Rolls-Royce PLC (London, GB)	An anti-icing system for an engine section stator of a gas turbine engine. The system includes an environmental control system pre-cooler heat exchange system and a conduit. The environmental control system pre-cooler heat exchange system is configured to exchange heat between air bled from a compressor of the engine and bypass duct air. The conduit is configured to exchange heat from the pre-cooler heat exchange system to a heat transfer medium. The conduit is also configured to transfer the heat from the heat transfer medium to the engine section stator.
9845418	2014	2017	HRL Laboratories LLC (Malibu, CA, U.S.)	Transparent, impact-resistant, anti-icing coatings are disclosed. In some variations, a transparent anti-icing coating comprises: a continuous matrix of a hardened material; asymmetric templates that inhibit wetting of water, wherein the asymmetric templates have a length scale from about 10-300 nanometers; porous voids surrounding the asymmetric templates, wherein the porous voids have a length scale from about 15-500 nanometers; and nanoparticles that inhibit heterogeneous nucleation of water, wherein the nanoparticles have an average size from about 5-50 nanometers. Disclosed coatings have transparencies of 90% or higher light transmission. These coatings utilize lightweight and environmentally benign materials that can be rapidly formed into coatings. A uniform distribution of particles and asymmetric templates throughout the coating allows it to be abraded yet retain its anti-icing function as well as transparency. Therefore, if the surface is damaged during use, freshly exposed surface is identical to that which was removed, for extended lifetime.
9794663	2016	2017	Symbol Technologies LLC	An ice-resistant speaker is provided. The ice-resistant speaker can be incorporated into a device comprising a housing having an outer surface and an inner surface opposite the outer

Patent No.	Year Filed	Year Granted	Assignee	Abstract
			(Lincolnshire, IL, U.S.)	surface. The ice-resistant speaker comprises: an audio port at the housing, the audio port comprising: a cavity at the outer surface of the housing; an aperture through the housing, the aperture located in the cavity; and a speaker pill located in the cavity and forming a gap with sidewalls of the cavity, the speaker pill mounted in front of the aperture using one or more flexible pads; and, a speaker driver located adjacent the inner surface of the housing, and further adjacent the aperture.
9683885	2015	2017	BAE Systems Information and Electronic Systems Information Inc. (Nashua, NH, U.S.)	An infrared countermeasure system comprises a transparent infrared camera dome with an anti-icing surface coating.
10000678	2015	2018	Gamesa Innovation and Technology, S. L. (Sarriguren (Navarra), ES)	Ice-resistant paint comprising an ice-resistant base component that in turn comprises a main component entailing a high solid paint with a synthetic polyurethane-based binding component dissolved in a main organic solvent, and a hydrophobe component consisting of hydrophobic ice-resistant functional nanoparticles selected from among nanoparticles functionalized with a polymer and nanoparticles functionalized in sol-gel, where the ice-resistant paint comprises a mixture of the main component with a dispersion of functional nanoparticles dispersed in a dispersing composition constituting the main solvent and a dispersant, and forms a base matrix, where the dispersing composition and functional nanoparticles form a dispersion of nanoparticles in which the functional nanoparticles are in the base matrix, and the dispersion of dispersing nanoparticles mixed with the main component to form an ice-resistant base component of the ice-resistant paint.
8221644	2011	2012	Miller Chemical	Methods are provided which minimize loss of an anti-icing/deicing composition from a

Patent No.	Year Filed	Year Granted	Assignee	Abstract
			and Fertilizer Corp. (Hanover, PA, U.S.)	surface. This is accomplished by adhering the anti-icing/deicing composition to a surface using a film-forming polymeric composition. Methods are also provided for preventing snow accumulation and/or ice formation on a surface, delaying ice and/or snow formation on a surface, extending the life of an anti-icing/deicing composition on a surface, surface anti-icing, and surface deicing. These methods include the application of a film-forming polymeric composition and the anti-icing/deicing composition to the surface. Desirably, the anti-icing/deicing composition is a reagent which reduces the freezing point of water.
8647709	2007	2014	Michigan Technological University, Houghton, MI (US)	A method of inhibiting or preventing bonding between snow or ice and a substrate. The method includes applying an adhesive to the substrate, broadcasting an aggregate onto the adhesive, the aggregate having the capacity to receive an anti-icing chemical into the aggregate, and applying the anti-icing chemical onto the aggregate so that at least a portion of the anti-icing chemical is received into at least a portion of the aggregate.

Patent No.	Year Filed	Year Granted	Assignee	Abstract
7883609	2002	2011	The Trustees of Dartmouth College (Hanover, NH, U.S.)	An alternating electric field is applied to ice (530) to generate a resistive AC having a frequency greater than 1000 Hz in interfacial ice at interface (554). A first electrode (510) and a second electrode (514) proximate to the interface are separated by an electrical insulator (512). An AC power source (520) provides a voltage of about 10 to 500 volts across the electrodes to create the alternating electric field. A portion of the capacitive AC associated with the alternating electric field is present in the interfacial ice as conductivity (resistive) AC, which causes dielectric loss heating in the interfacial ice.

Patent No.	Year Filed	Year Granted	Assignee	Abstract
7981313	2010	2011	BASF SE (Ludwigshafen, DE)	The use of hydrophobics for preventing the formation of ice on surfaces, especially for the prevention of ice formation on aircraft surfaces.
8395504	2007	2013	Toppan Printing Co. Ltd. (Tokyo, JP), Hitachi. Ltd. (Tokyo, JP)	An IC label for prevention of forgery includes: a label substrate which has an adhesive agent for affixing the same to an object; a non-contact IC medium which is provided on the label substrate and has an IC chip for storing predetermined identification information and an antenna for wireless transmission of the identification information; and a security function portion which is provided on the label substrate and prevents replication.
6211493	2000	2001	Bouman, Geni F. (Port Lambton, Ontario, CA)	An ice prevention mat system that includes multiple resilient electrically heatable mats that are positionable to cover a desired pathway and which includes a control circuit for maintaining each of the electrically heatable mats at a temperature sufficient to melt snow falling on the mat as well as to prevent the formation of ice on the mat top surface. Each of the multiple resilient electrically heatable mats has a top surface partially covered a non-skid or slip coating as well as light assemblies along the side borders to clearly identify the side edges of the mats.
Patent No.	Year Filed	Year Granted	Assignee	Abstract
8851858	2011	2014	GE Aviation Systems Ltd. (Gloucestershire, GB)	A propeller blade for rotation about a hub assembly is provided, wherein the propeller blade defines a radial direction along its length from a blade root to a blade tip, the propeller blade including a radially inner region, a radially outer region located between the blade root and the blade tip at a position where rotational forces on the blade are sufficient, in use, to remove ice from an uncoated blade, a coating disposed at least along a leading edge of the propeller blade, the coating including an icephobic material, wherein the coating extends along

Patent No.	Year Filed	Year Granted	Assignee	Abstract
				the propeller blade from the radially inner region to the radially outer region.
9546280	2012	2017	HRL Laboratories LLC (Malibu, CA, U.S.)	Variations of this invention provide durable, impact-resistant structural coatings that have both dewetting and anti-icing properties. The coatings in some embodiments possess a self-similar structure that combines a low-cost matrix with two feature sizes that are tuned to affect the wetting of water and freezing of water on the surface. Dewetting and anti-icing performance is simultaneously achieved in a structural coating comprising multiple layers, wherein each layer includes (a) a continuous matrix; (b) discrete templates dispersed that promote surface roughness to inhibit wetting of water; and (c) nanoparticles that inhibit heterogeneous nucleation of water. These structural coatings utilize low-cost, lightweight, and environmentally benign materials that can be rapidly sprayed over large areas using convenient coating processes. The presence of multiple layers means that if the surface is damaged during use, freshly exposed surface will expose a coating identical to that which was removed, for extended lifetime.
9260629	2010	2016	United Technologies Corp. (Hartford, CT, U.S.)	A coated article includes a substrate and a superhydrophobic coating on the substrate. The superhydrophobic coating is a composite of a silicone polymer and particles that are inherently hydrophobic or surface-functionalized with a hydrophobic agent
9862881	2016	2018	Preferred Technology LLC (Radnor, PA, U.S.)	Compositions and methods for coated or uncoated particulates, such as proppants, are provided that can, among other things, provide a hydrophobic surface that can enhance well productivity and other compositions and methods are disclosed.
9199741	2014	2015	The Boeing Co. (Seal Beach, CA, U.S.)	Global icephobic performance of a passive deicing structure may be achieved by including one or more ice nucleating zones

Patent No.	Year Filed	Year Granted	Assignee	Abstract
				that are configured, preselected, and/or arranged to promote selective formation of ice. Ice nucleation zones may be configured, preselected, and/or arranged to form ice that is weakly adherent and, hence, may be removed by sufficient shear force. Ice nucleation zones typically include nucleating particles to promote selective ice formation. Passive deicing structures typically include both ice nucleation zones and ice resisting zones, arranged to facilitate ice removal by shear force. Passive deicing structures may be used on apparatuses such as vehicles (e.g., aircraft) to mitigate the effects of ice formation on exposed surfaces.
8221847	2008	2012	Berman Joan, Lycron Arrakis LLC (Cheyenne, WY, U.S.)	The present invention provides a method for providing anti-ice protection to surfaces, particularly aerodynamic surfaces, to prevent foul weather icing for extended periods of time and over repeated icing situations, comprising applying an organic polymer matrix layer to the surface where the organic polymer matrix layer comprises a homopolymer comprising up to 50% porous polymer solids having a pore size of up to 100 Angstroms and being capable of absorbing and chemically bonding an aqueous freeze-point depressant solution in amounts of up to 99.75% by weight.

DISTRIBUTION

Email—Internal

Name	Org.	Sandia Email Address
Nelson S. Bell	01815	nsbell@sandia.gov
Gary S. Grest	01881	gsgrest@sandia.gov
Hannah Narcross	01815	hnarcro@sandia.gov
Technical Library	1911	sanddocs@sandia.gov

This page left blank

Sandia National Laboratories

Sandia National Laboratories is a multimission laboratory managed and operated by National Technology & Engineering Solutions of Sandia LLC, a wholly owned subsidiary of Honeywell International Inc. for the U.S. Department of Energy's National Nuclear Security Administration under contract DE-NA0003525.